

Rheology of Bitumen at the Onset of Asphaltene Aggregation and its Effects on
the Stability of Water-in-Oil Emulsion

by

Saeed Mozaffari

A thesis submitted in partial fulfillment of the requirements for the degree of

Master of Science
in
Chemical Engineering

Department of Chemical and Materials Engineering
University of Alberta

© Saeed Mozaffari, 2015

Abstract

Asphaltenes are the heaviest fraction of bitumen. Asphaltenes not only play an important role in the high viscosity of bitumen but also in the water-in-oil (W/O) emulsion stability. Nevertheless, their exact function in the stability mechanism of W/O emulsion still remains unresolved. It is observed that asphaltenes are very inclined to form aggregates in organic solvents, especially in aliphatic solvents. The existence of such aggregates alters the rheological properties of bitumen in macro-and nanoscale. In this thesis, the focus of the study is on the role of asphaltenes aggregation on rheological properties of diluted bitumen. The influence of solvents with different degree of aromaticity on asphaltenes aggregation/precipitation is further investigated. Further, nanofluidic chips are designed and fabricated to enable us to inspect the fluid properties (such as penetration, velocity, and viscosity) in the nano-confinement geometry. Capillary-driven flow is used to transport pure solvents and diluted bitumen (with or without the presence of asphaltenes aggregation). Finally, theoretical predictions are applied to analyze and compare the data with the experimental values based on capillary filling phenomena.

To my parents, brothers, sister and nephews for their everlasting
love, support and encouragement.

Acknowledgments

First and foremost, I would like to express my gratitude to my great supervisors and mentors, Dr. Neda Nazemifard and Dr. Jan Czarnecki, for their intellectual support, encouragement, and granting me freedom to explore my ideas. I really have no words to thank Dr. Plamen Tchoukov my advisor and friend for his guidance, technical support, and friendship that made my research fruitful and fun.

Next, I wish to express my appreciation to Dr. Amir Afshar for helping me out during my moments of desperation and frustration- without his help I would not be encouraged to pursue a higher education. I also would like to thank Dr. Zhenghe Xu for kindly allowing me to use their lab equipment.

I would like to thank Dr. Tony Yeung, Dr. Hyun-Joong Chung, and Dr. Dominic Sauvageau, my examining committee members.

I gratefully acknowledge the financial support from Natural Sciences and Engineering Council of Canada (NSERC) and Dow Chemical Canada, which assisted me throughout my studies.

Gratitude is also expressed to my supportive lab members- Kiarash, Muhammad, Gunjan, Swapnali, and Kevan. I would like to extend my thanks to my great friends- Sadegh, Ali, Mohsen, Ehsan, Mohammad, Hafez, Pouya, Alireza, Montazar, Mostafa, Moien, Negar, Hadie, Mahdie, Lin, Lily, Marion, Siddhant, Lotf, Ammi, Hesam, Hasson, and Eskandar for their invaluable companionship.

At last, I would like to thank my family members, especially my mother Ziba and my nephews Shayan and Mohammad Reza for being an asset in my life. A special thank goes to Homa back home for her continuous support, and encouragement. I am very lucky to have such fantastic companions in my life.

Table of Contents

Chapter 1: General Introduction.....	1
1.1 Introduction.....	1
1.2 Research Objectives	6
1.3 Thesis Layout.....	7
Chapter 2: Effect of Asphaltenes Aggregation on Bitumen Rheology	9
2.1 Introduction.....	9
2.2 Experimental Section	14
2.2.1 Materials	14
2.2.2 Solutions Preparation and Procedures	15
2.2.3 Bitumen Content Measurement.....	15
2.2.4 Viscosity Measurements	15
2.3 Results and Discussion.....	17
2.3.1 Viscosity of Aged Diluted Bitumen Solutions	17
2.3.2 Bitumen Content of Supernatant of Aged Solutions	20
2.3.3 Newtonian Behavior of Bitumen Solutions	21
2.4 Theoretical Section.....	25
2.4.1 Effective Volume Fraction of Dispersed Bitumen and Asphaltenes	25
2.4.2 Effective Volume Fraction of Dispersed Bitumen	27
2.4.3 Volume Fraction of Dispersed Asphaltenes.....	28
2.5 Conclusion	30
Chapter 3: Nanofluidic Devices for Rheology Analysis of Diluted Bitumen.....	32
3.1 Introduction.....	32
3.2 Experimental Section.....	36
3.2.1 Nanofabrication.....	36
3.2.2 Materials	39
3.2.3 Bitumen Samples Preparation and Procedure.....	39
3.2.4 Viscosity Measurements	40
3.2.5 Surface Tension and Bulk Contact Angle Measurements	40
3.2.6 Position and Speed of Moving Liquid Meniscus	41
3.3 Theory	41
3.3.1 Newtonian Fluid	41

3.3.2 Non-Newtonian Bingham Plastic Fluid	43
3.4 Results and Discussion	44
3.4.1 Capillary-Driven Flow of Pure Liquids	44
3.4.2 Capillary-Driven Flow of Bitumen Solutions	50
3.4.3 Capillary-Driven Flow of Bingham Plastic Fluid	59
3.5 Conclusion	63
Chapter 4: Conclusions and Future Work.....	65
4.1 Concluding Remarks	65
4.2 Future Work.....	68
References	71
Appendix A: MATLAB Code for Solving Equation (9) Presented in Chapter 3	84

List of Tables

Table 2.1 Summary of Critical S/B Ratio for Different Solvents	11
Table 3.1 The Values of Different Liquids Physical Properties	59

List of Figures

Figure 2.1 Formation of asphaltene cluster from its molecule.....	10
Figure 2.2a A molecular structure of an anionic surfactant known as Sodium Dodecyl Sulfate (SDS).....	13
Figure 2.2b A molecular structure of asphaltene.....	13
Figure 2.3 (a) Rheometer and (b) Concentric cylinder geometry	16
Figure 2.4 Viscosity of bitumen diluted in heptol (80:20) as a function of aging time. The errors in viscosity measurements are less than 0.008 mPa·s.	18
Figure 2.5 Viscosity of bitumen diluted in heptane as a function of aging time. The errors in viscosity measurements are less than 0.008 mPa·s.	19
Figure 2.6 The bitumen content and volume fraction of 11 wt.% bitumen diluted in heptol (80:20) and heptane as a function of aging time	21
Figure 2.7 Shear stress versus shear rate for 5 wt.% bitumen in heptol (80:20). Sample was centrifuged at 16,000 g for 60 min with 7 days aging time.	23
Figure 2.8 Shear stress versus shear rate for 5 wt.% bitumen in heptane. Sample was centrifuged at 16,000 g for 60 min with 7 days aging time	24
Figure 2.9 Shear stress versus shear rate for 11 wt.% bitumen in different solvents. Samples were centrifuged at 16,000 g for 60 min with 0 day aging time.	25
Figure 2.10 Effective volume fraction of bitumen in different solvents as a function of aging. The errors in the estimated volume fraction are less than 0.006	28
Figure 2.11 Volume fraction of asphaltenes as a function of aging in bitumen solutions. The errors in the estimated volume fraction are less than 0.008	29
Figure 2.12 Volume fraction of asphaltenes as a function of aging in bitumen solutions. The errors in the estimated volume fraction are less than 0.009	30
Figure 3.1 Etching depth as a function of etching time using reactive ion etching (RIE).	38
Figure 3.2 Schematic of nanochannels fabrication	38
Figure 3.3 AFM image of centimeter long, 15 μm wide, and 47 nm deep	

channel etched by RIE. The mean roughness (Ra) was determined to be 0.6 nm	39
Figure 3.4 Capillary filling of a liquid in the horizontal channel.....	42
Figure 3.5 The Penetration of pure liquids as a function of $t^{0.5}$ in nanochannel with the depth and width of 47 nm and 15 μm , respectively	47
Figure 3.6 The variation of theoretical viscosity for ethanol as a function of penetration distance in nanochannel with the depth and width of 47 nm and 15 μm , respectively.....	48
Figure 3.7 The variation of x/k as a function of $t^{0.5}$ for capillary flow of pure liquids in nanochannel with the depth and width of 47 nm and 15 μm , respectively	49
Figure 3.8 The velocity of advancing liquids as a function of penetration distance in nanochannel with the depth and width of 47 nm and 15 μm , respectively	50
Figure 3.9 The Penetration of bitumen solutions diluted in heptol (80:20) as a function of $t^{0.5}$ in nanochannel with the depth and width of 47 nm and 15 μm , respectively.....	53
Figure 3.10 The variation of x/k as a function of $t^{0.5}$ for capillary flow of bitumen solutions diluted in heptol (80:20) in nanochannel with the depth and width of 47 nm and 15 μm , respectively.....	54
Figure 3.11 Empty reservoir before filling with 40% bitumen.	55
Figure 3.12 Capillary filling of 40 wt.% bitumen diluted in heptol (80:20) at $t= 0.3$ s	55
Figure 3.13 Capillary filling of 40 wt.% bitumen diluted in heptol (80:20) at $t= 1.4$ s.....	56
Figure 3.14 Capillary filling of 40 wt.% bitumen diluted in heptol (80:20) at $t= 6.7$ s.....	56
Figure 3.15 Formation of air bubbles during capillary filling of 20 wt.% bitumen diluted in heptol (80:20).....	57

Figure 3.16 The velocity of advancing bitumen solutions diluted in heptol (80:20) as a function of penetration distance in nanochannel with the depth and width of 47 nm and 15 μm , respectively	58
Figure 3.17 The measured bulk contact angle of 40 wt.% bitumen in heptol (80:20) on borofloat glass 0.3 s after the contact. The mean contact angle was about 26 degree.....	58
Figure 3.18 The measured bulk contact angle of 5 wt.% bitumen in heptol (80:20) on borofloat glass 0.3 s after the contact. The mean contact angle was about 12 degree.....	59
Figure 3.19 Schematic of thin oil film drainage from W/O emulsion study.....	61
Figure 3.20 The theoretical prediction of Bingham Plastic flow penetration as a function of $t^{0.5}$ distance in nanochannel with the depth and width of 47 nm and 15 μm , respectively	62
Figure 3.21 The theoretical prediction of Bingham Plastic velocity as a function of penetration distance in nanochannel with the depth and width of 47 nm and 15 μm , respectively	63

List of Symbols

η_r	relative viscosity
k_0	Einstein constant
k_1	Huggins constant
ϕ	volume fraction
ϕ_{\max}	maximum volume fraction packing of particles
K'	solvation coefficient
w	channel width (m)
h	channel height (m)
z	half of channel height (m)
x	penetration distance (m)
P	pressure (Pa)
μ_f	fluid viscosity (Pa.s)
μ_B	Bingham fluid viscosity (Pa.s)
V_x	fluid velocity (m/s)
σ	air-liquid surface tension (N/m)
θ_c	liquid advancing contact angle (°)
θ_b	bulk contact angle (°)
t	time (s)
τ_{yx}	shear stress (Pa)
τ_0	Bingham yield stress (Pa)

Chapter 1: General Introduction

1.1 Introduction

An emulsion is a mixture of two immiscible liquids which is thermodynamically unstable, even though kinetically stable.^{1, 2} Emulsions have found enormous applications in food, pharmaceutical, and cosmetic industries.³ However, emulsions are not always desirable. Formation of very stable water-in-crude oil emulsions is a major problem in petroleum industry, and particularly in the recovery of bitumen from the vast resource of oil sands in Alberta. During heavy/crude oil production, vigorous agitation when the oil flows through wellbores, valves, and pump impellers, along with the presence of indigenous natural surfactants, asphaltenes and fine solids, emulsify some water into small droplets.

Presence of salt in water droplets can cause severe problems such as corrosion of pipelines and refinery equipment.^{4, 5} Emulsified water droplets can add up to the viscosity of crude oil leading to a significant increase in the cost of pumping, transportation, and lead to a possible environmental damage.^{2, 6} Large water droplets can be easily removed using standard gravitational settling or centrifugation methods, the few micron-sized droplets however, are difficult to separate.

Due to the presence of various species in the bitumen or heavy crude oil, W/O emulsion becomes stabilized.⁷ Interestingly, the molecular mechanisms that determine the W/O emulsion stability are still unknown.² Acidic molecules

present in the crude oil contribute in the stability of W/O emulsion.² These acidic molecules are capable of ionization at the W/O interface and can considerably lower the interfacial tension.^{8, 9} Some of these stabilizing acids are alkyl carboxylic acids, fused aromatic ring acids, alkylbenzene carboxylic acids, and naphthenic acids.²

Fine inorganic solid particles, such as clays, silicas, and iron oxides are found to engage in the stabilization of W/O emulsion through surface modification. Crude oil species like resins and asphaltenes can be adsorbed at the surface of small inorganic particles, therefore; make the small particles interfacially active.²

Asphaltenes as the heaviest fraction of bitumen are widely acknowledged to play a critical role in the stability mechanism of W/O emulsion.^{7, 10} Asphaltenes are considered as one of the main mechanisms for stabilization of W/O emulsion. Despite numerous scientific studies to elucidate how asphaltenes contribute to the stability mechanism, their exact role is not well-understood.¹¹ Asphaltenes are weak surface-active agents that cannot lower the interfacial tension as other bitumen fractions like resins.¹² Moreover, asphaltenes mostly consist of hydrophobic part and does not possess a well-defined amphiphilic structure.¹¹ Therefore, asphaltenes cannot be considered as a type of surfactant.

Asphaltenes are defined as a solubility class of molecules that are soluble in toluene but insoluble in n-heptane or n-pentane.¹ Asphaltenes form aggregates even in aromatic solvents such as toluene.¹³ Asphaltene molecules initially form nano-aggregates and then nano-aggregates can evolve to larger structures, such as clusters and precipitates.^{11, 14} The presence of solid asphaltenes is associated

to various industrial problems such as catalyst deactivation, low distillate yields, equipment failure, and pipeline plugging.¹⁴⁻¹⁶

High viscosity of bitumen is mostly determined by the asphaltenes content and the interactions between asphaltenes and maltenes.¹⁷ The various techniques used to reduce the viscosity of bitumen/heavy oil include heating, addition of liquid diluents, steam injection, and emulsification.^{18, 19} Dilution is the most preferred method to reduce the bitumen viscosity.¹⁸ Therefore, use of light hydrocarbons is essential for facilitating bitumen transportation. Solvent aromaticity and degree of dilution are important parameters in the formation of asphaltenes aggregates.²⁰ There are clear evidences that at the critical solvent to bitumen ratio (S/B) asphaltenes aggregate and form large precipitates.²⁰⁻²² Regarding the role of asphaltenes in the stability of W/O emulsion, it is found that above the critical S/B ratio where asphaltenes precipitation takes place, sudden changes at the interfacial characteristic of W/O occur.^{21, 22} Below critical S/B ratio, the W/O interface is fluid while above the critical dilution rigid interface can be observed.^{21, 22} It is well-appreciated that at the W/O interface, asphaltenes are responsible for formation of viscoelastic layer.^{23, 24} The viscoelastic layer is mechanically strong and deemed to be a mechanism for stabilization of W/O emulsion.²⁴ Asphaltenes can aggregate with resin molecules at the interface and hinder water droplets to coalesce through steric repulsion and as a result enhance the emulsion stability.²⁵ It has been reported in few studies that asphaltene can form hydrogen bonds with water molecules and stabilize the emulsion.^{26, 27}

In the recent studies, it is observed that at the W/O interface stable and rigid oil film prevents two approaching water droplets to coalesce and form a larger water droplet.¹¹ Drainage of thin oil film stops at the thickness of less than 100 nm. This phenomenon was addressed to the formation of hierarchical asphaltene aggregation that changes oil rheology from Newtonian to non-Newtonian by inducing a tiny yield stress.¹¹ Therefore, it is of a great importance to further investigate how asphaltene affect the oil rheology under the nano-confinement geometry.²⁸

With the rapid advances in the field of nanotechnology, fabrication of nanostructure features became feasible. Due to the emergence of nanofluidics, numerous studies regarding transport phenomena in the nanoscale have been conducted. Modeling of transport phenomena inside nanofluidics is different from microfluidics as the effect of wall in the nanometer scale becomes more influential.²⁹ Nanofluidics is the study of fluid flow in the nanochannels/nanopores with at least one characteristic size below 100 nm.³⁰ High surface area to volume ratio, and comparable channel size with biomolecules like DNA and proteins are the distinctive characteristic of nanofluidic systems.³¹ Various applications of nanofluidics include single cell analysis³², water purification³³, DNA sensing³⁴, and energy conversion³⁵. To fabricate nanofluidic devices, several nanofabrication methods, such as photolithography, electron beam lithography (EBL), focused ion beam (FIB), nanoimprint lithography (NIL), and self-assembly have been used.^{31, 36, 37}

Nanochannels with different aspect ratio (AR) of cross sectional area can be fabricated, where AR is the ratio of height to width.³⁸ In one dimensional (1-D) nanochannels only one dimension (height or Width) is in the nanometer scale. However, in two dimensional (2-D) nanochannels both dimensions are in the nanometer scale.³⁸ Ultra low AR (i.e., $w \gg h$) nanochannels can be considered as 1-D systems which facilitates theoretical analysis.³⁹ Furthermore, 1-D nanochannels provide higher volumetric flow in comparison with 2-D nanochannels.⁴⁰

Electro-osmotic flow (EOF) is the preferred method for fluid transport inside the nanofluidic systems.²⁹ An interesting application of EOF systems is to separate the components of a mixture.⁴¹ However, one of the main limitation of this method is that it can be applied to the aqueous solutions.⁴² Pressure-driven flow is another method of fluid transport which can be used for any fluid type unlike EOF flow.⁴²

Owing to the large surface area to volume ratio in the nanoscale, surface-liquid interactions become important.⁴³ Therefore, capillary action in the nanofluidics is very prominent.⁴⁴ Furthermore, the wetting properties of channels wall play an important role in the spontaneous filling of liquid inside nanochannels.⁴⁵ The liquid filling kinetics through capillary action was first studied by Washburn.⁴⁶ Several studies demonstrated that liquid filling speed in the nanochannels deviates from the theoretical predictions.^{43, 44, 47} Such deviation was attributed to the variation in dynamic contact angle^{43, 48}, or to the electro-viscous effect⁴⁴. Fluid transport inside the nanofluidic system can provide an insight into the

effect of nano-confinement on the fluid viscosity and other rheological properties. In this regard, capillary-driven flow is a promising method to analyze the flow of complex fluids in the nanoscale. Further, this method can be applied to study the flow of heavy crude oil and bitumen inside nanoporous media.

1.2 Research Objectives

Bitumen is an organic material with a complex molecular structure. Bitumen is also a mixture of diverse hydrocarbons in which their properties are very similar.⁴⁹ Due to the complex chemistry of bitumen, bitumen chemical structure is not yet precisely determined. In the petroleum industry, there is a standard method to classify bitumen fractions into four groups. Saturates, Aromatics, Resins, and Asphaltenes are the four distinct fractions of bitumen known as SARA classification.⁵⁰

Asphaltenes are the most studied components of heavy crude oil and bitumen. Asphaltenes are still the least understood fraction of bitumen.⁵¹ As already mentioned in the introduction part, asphaltenes are the most aromatic and the heaviest components of bitumen and heavy crude oil.¹¹ Asphaltenes have large applications in paving, coating, and encapsulation of hazardous waste.⁵² On the other hand, negative impacts of asphaltenes on the petroleum industries are emulsion stabilization, low production yield, and bitumen high viscosity.¹⁴

The first objective of this study is to understand how time evolution of asphaltenes aggregation/precipitation affects the viscosity of diluted bitumen. Efficiency of centrifugation on asphaltenes removal and viscosity was also analyzed. Furthermore, different types of solvent were used to investigate how

solvents with different degree of aromaticity alter the rate of asphaltenes aggregation/precipitation.

The second objective of this thesis is to design and fabricate a nanofluidic chip for in-situ monitoring of the filling kinetics of various pure solvents and mixtures. High speed camera was used to trace the position of advancing liquid with time and a labview program to record the data. Experiments have been conducted with various bitumen concentrations above and below critical S/B ratio in the nano-confinement geometry.

Finally, nanofluidic chip was utilized to examine the impact of asphaltenes aggregation on the diluted bitumen rheology. Furthermore, theoretical predictions were developed to make a comparison with the experimental data.

1.3 Thesis Layout

The work in this thesis is divided into four chapters. In Chapter 1 (the current chapter), a general overview of asphaltenes role in the stability mechanism of W/O emulsion, and also in bitumen rheology (in both macro-and nanoscale) have been demonstrated. Afterwards, the main objectives and scope of this research have also been presented.

Chapter 2 is focused on the effect of asphaltenes aggregation on the rheological properties of bitumen. In the introduction part, a brief definition of asphaltenes and their contribution in the bitumen viscosity have been presented. Further, by considering asphaltenes as colloidal dispersion of particles, viscosity modeling was performed to estimate the volume fraction of bitumen and asphaltenes in the

mixture. The use of such viscosity modeling can be helpful to estimate some limited values which may not be possible experimentally.

In chapter 3, a detailed literature review on the application of nanofluidic devices, their unique features, and the main methods of fluid transport in these miniaturized devices have been discussed. The procedure and schematic for fabrication of nanofluidic chip and further surface analysis were demonstrated.

A description of capillary-driven flow as the method of fluid transport in our experiments was given. The method for bitumen sample preparation above and below the critical S/B ratio was established. We tried to examine a possible role of asphaltenes in diluted bitumen rheology when aggregates formed in the nano-confinement geometry. Furthermore, theoretical prediction was used to inspect the filling kinetics of Newtonian and non-Newtonian Bingham fluid.

Finally, in Chapter 4, we summarize the major findings of the conducted research and propose some directions and suggestions for the future investigations.

Chapter 2. Effect of Asphaltenes Aggregation on Bitumen Rheology

2.1 INTRODUCTION

Asphaltenes cause severe problems in the heavy crude oil transportation, oil recovery, water removal, and catalyst efficiency.^{4, 15, 16, 21, 23, 53-55} Asphaltenes are defined as a fraction of crude oil that is soluble in toluene and insoluble in pentane or heptane.⁵⁶ As a solubility class the asphaltenes consist of large variety of molecules² which are different almost in any kind of property, such as molecular weight, functional groups and polarity, and only their solubility behavior in aromatic and aliphatic solvents are similar.^{11, 14, 15} Furthermore, the asphaltene content is the parameter that affects the viscosity of bitumen.^{57, 58} Bitumen is the residue of a refining process in the petroleum industry which mainly originates from the crude oil. Bitumen is a complex material that its viscosity is very temperature dependent.⁵⁹ Bitumen fractions based on SARA classification are categorized into four groups of Saturates, Aromatics, Resins, and Asphaltenes. These fractions are different in several properties, such as molecular weights, hydrogen to carbon ratio (H/C), and polarity.⁵⁰ Asphaltenes have a density between 1.1–1.2 g/cm³ and H/C ratio of 1.1–1.2 at the room temperature.⁶⁰

A version of this chapter has been submitted to the journal of Energy & Fuels and is under review for publication.

Asphaltenes are solids, shiny and black. Asphaltenes as the largest and heaviest fraction of bitumen are known for their high tendency to form aggregates.^{11, 14, 61} Aggregation mechanism of asphaltenes is responsible for reduction of asphaltenes diffusivity.⁶²

The aggregation number of nano-aggregates is reported to be less than 10.¹⁴

It has been a long debate on determination of asphaltene molecular weight. Recently, the asphaltene average molecular weight was reported to be around 750 Da.⁶²

Bouhadda et al.⁶³ based on viscosity results found that asphaltenes form spherical aggregates in toluene solution at volume concentration up to 0.15. Eyssautier et al.⁶² by using small angle neutron and X-ray scattering techniques proposed a disk shape model for asphaltene nano-aggregates. The aggregation of asphaltenes is not limited only to nano-aggregates but is rather a hierarchical process that includes formation of nano-aggregate clusters and large precipitate particles.¹⁴ Asphaltene clusters consist of nano-aggregates. The evolution of asphaltene growth from its molecule to form cluster is shown in Figure 2.1.

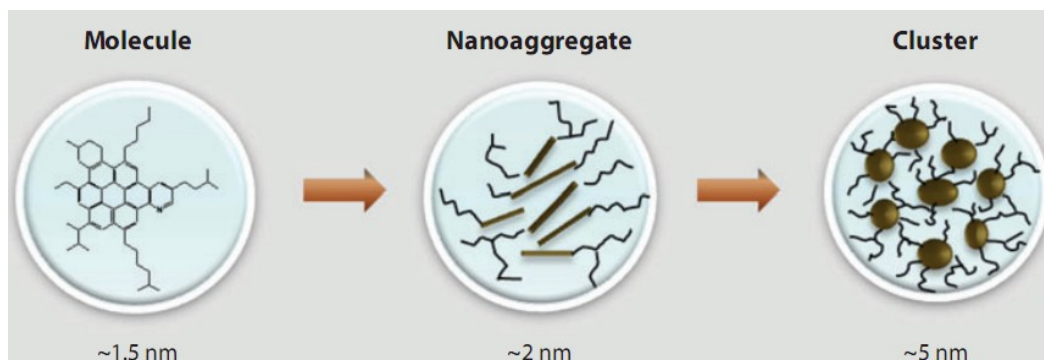


Figure 2.1. Formation of asphaltene cluster from its molecule.¹⁴

In order to enhance water and solids removal or to facilitate transportation of bitumen, an addition of light hydrocarbon is required to reduce the viscosity and density of bitumen. Solvent to bitumen ratio (S/B) and solvent composition (aromaticity) have a profound impact on the formation of asphaltene aggregates.^{20, 53} There is a critical S/B, at which an apparent asphaltene precipitation is observed.²⁰⁻²² The observation of asphaltene aggregates and their precipitation have been originated from the study of W/O emulsion.^{20, 21} In this regard, there is a transition from fluid to rigid interface at the onset of asphaltene precipitation. The results of critical S/B ratio (thick line) for different solvents are summarized by Tchoukov et al.²⁰ and shown in Table 2.1.

S/B	1	2	3	4	9	19	32.3	99
Bitumen wt. %	50%	33%	25%	20%	10%	5%	3%	1%
Heptane	FL	RG	RG		RG			
Heptol (80:20)	FL	FL	RG	RG	RG	RG		
Heptol (50:50)	FL		FL	FL	FL	FL	RG	RG
Toluene	FL	FL	FL	FL	FL		FL	

Table 2.1. Summary of critical S/B ratio for different solvents.²⁰

The rate and degree of the asphaltene aggregation/precipitation is determined by the asphaltene solubility properties in the used solvent. Pressure, temperature, phase separation, and variations in the composition are the key parameters that enhance the asphaltene precipitation.

Sheu¹⁵ reported the effect of aging on the viscosity of 2.1 wt.% asphaltenes in heptane/toluene (25:75) solution. Viscosity increase of about 30% was noticed after 400 min aging. This change in the viscosity was addressed to the flocculation of asphaltenes. Similarly, molecular dynamic study suggested that as the bitumen ages, asphaltenes aggregation develops and bitumen viscosity increases.⁵⁰ Recently, Tchoukov et al.¹² compared the viscosity of asphaltenes, maltenes and bitumen in toluene solutions in the concentration interval 0–100 g/L and found that the asphaltenes content determines the viscosity of bitumen to a large extent. Eyssautier et al.⁶⁴ investigated the rheological behavior of asphaltenes in toluene in the concentration range from 0 to 20.0 vol % at temperatures between 80 and 240°C and found a Newtonian fluid behavior for all samples.

It has been well-supported in a number of studies that asphaltenes play a crucial role in the stability of water-in-crude oil (W/CO) emulsions.^{1, 21, 65, 66} The role of asphaltenes aggregation on rheological properties of oil and W/CO emulsions has been extensively studied.^{12, 16, 24, 58, 64}

It is important to note that asphaltenes molecular structure is different from a surfactant. Asphaltenes do not have a well-defined hydrophilic and hydrophobic part in their structure which is the characteristic of a surfactant.¹¹ A typical molecular structure of a surfactant and asphaltene are shown in Figure 2.2a and Figure 2.2b.

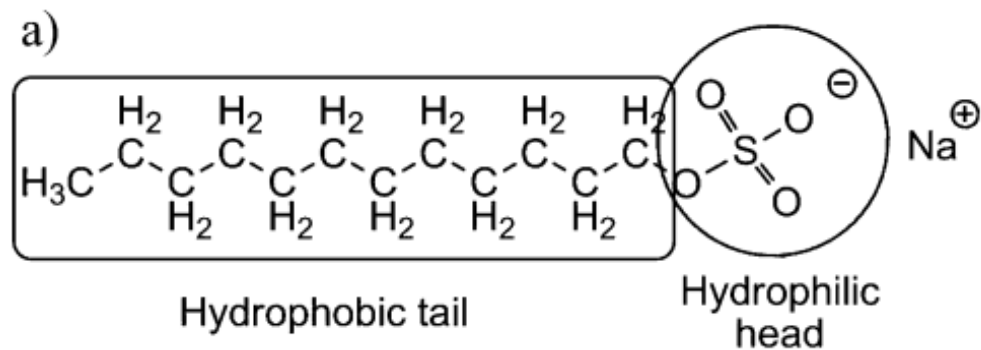


Figure 2.2a. A molecular structure of an anionic surfactant known as Sodium Dodecyl Sulfate (SDS).¹¹

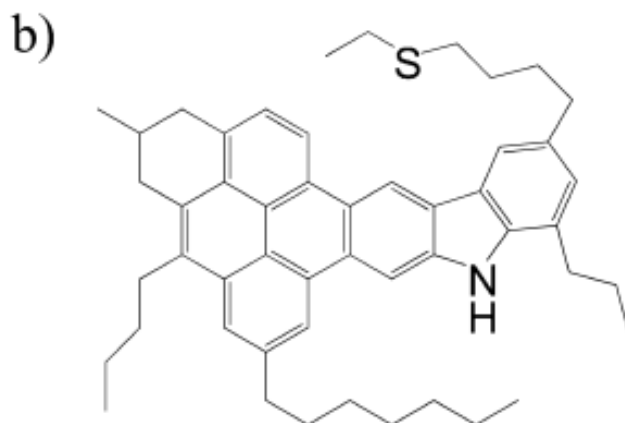


Figure 2.2b. A molecular structure of asphaltene.¹¹

To address the role of asphaltenes in the stability mechanism of W/O emulsion, Spiecker et al.²⁴ pointed out that the formation of asphaltene film at oil-water interface exhibits viscoelastic behavior and yield stress. Studying the drainage of the oil films between water droplets, Czarnecki et al.^{11, 67} proposed that in proximity of water/oil interface the asphaltenes can form not only small aggregates but also a supra-molecular network structure that changes the

rheological properties of the film liquid from Newtonian to non-Newtonian with a finite yield stress.

Despite the fact that a number of studies report data on viscosity of diluted bitumen at different concentration, temperature and pressure, until now, the effects of aging and asphaltenes aggregation have not been studied systematically. In order to investigate the effects of aging and S/B ratio on rheological properties of diluted bitumen we studied solutions at concentrations above and below the critical S/B. One day after preparation, the solutions were centrifuged to remove the initially formed precipitates and any fine solids that might be present; then the solutions were left to age for different times - up to 30 days when the viscosity of the supernatant was measured. Finally, based on viscosity models available in the literature, the effective volume fractions of bitumen and asphaltenes were evaluated.

2.2 EXPERIMENTAL SECTION

2.2.1. Materials

Athabasca coker feed bitumen supplied by Syncrude Canada Ltd was used in this work. The bitumen was diluted with n-heptane (HPLC grade Fisher Scientific), toluene (Optima, Fisher Scientific), and a mixture of heptane and toluene at the volume ratio of 80:20, which is referred in the text as heptol (80:20). The heptol (80:20) was selected because it has similar solubility properties to commercial naphtha used in froth treatment by Syncrude Canada Ltd.

2.2.2. Solutions Preparation and Procedures

Stock solutions of 50 wt.% bitumen in toluene, heptane and heptol (80:20) were used to prepare solutions with concentrations 5 – 45 wt.% in the studied solvents. Freshly prepared solutions were allowed to age for one day. The supernatants were collected and centrifuged at 16,000 g for 60 min at room temperature to ensure that all precipitates and fine solids are removed. After that the centrifuged solutions were aged for 0, 2, 7, or 29 days (the total aging time is 1, 3, 8, and 30 days) and used in viscosity and bitumen content measurements. To investigate the efficiency of centrifugation for removal of the initial precipitates in the solutions we conducted experiments with 5 and 11 wt.% bitumen in heptol (80:20) and heptane solutions, which were aged for 15 min and centrifuged at 16,000 g for 60 and 180 min. The different centrifugation time did not lead to any change in the measured viscosity of the samples.

2.2.3. Bitumen Content Measurement

The bitumen content of the samples aged for different time was estimated by taking 2 mL solution from the middle of the vial and spraying it on a filter paper (Grade 5, GE Healthcare Life Sciences). The filter papers were left under a fume hood for 15 min (the weight did not change if longer time was used) to evaporate the solvent. The net weight of dry bitumen was used to calculate the bitumen content of the samples.

2.2.4. Viscosity Measurements

Viscosity measurements were performed by using ARG2 rheometer (TA Instrument) in Flow Sweep Mode. Peltier concentric cylinder system was

selected as this geometry is more compatible with low viscosity measurements. The operating gap was set to 5917.1 μm . The equilibration time in steady state sensing was 5 seconds. Viscosity and shear stress were measured by varying shear rate from 1 to 150 s^{-1} . The experiments were repeated three times to ensure the accuracy of the measurements. For all experiments the temperature was set to 23 ± 0.02 $^{\circ}\text{C}$. Pure solvents with a known viscosity, such as water, heptane, and toluene were used to calibrate the viscosity measurements. The schematic of rheometer and concentric cylinder geometry are illustrated in Figure 2.3.

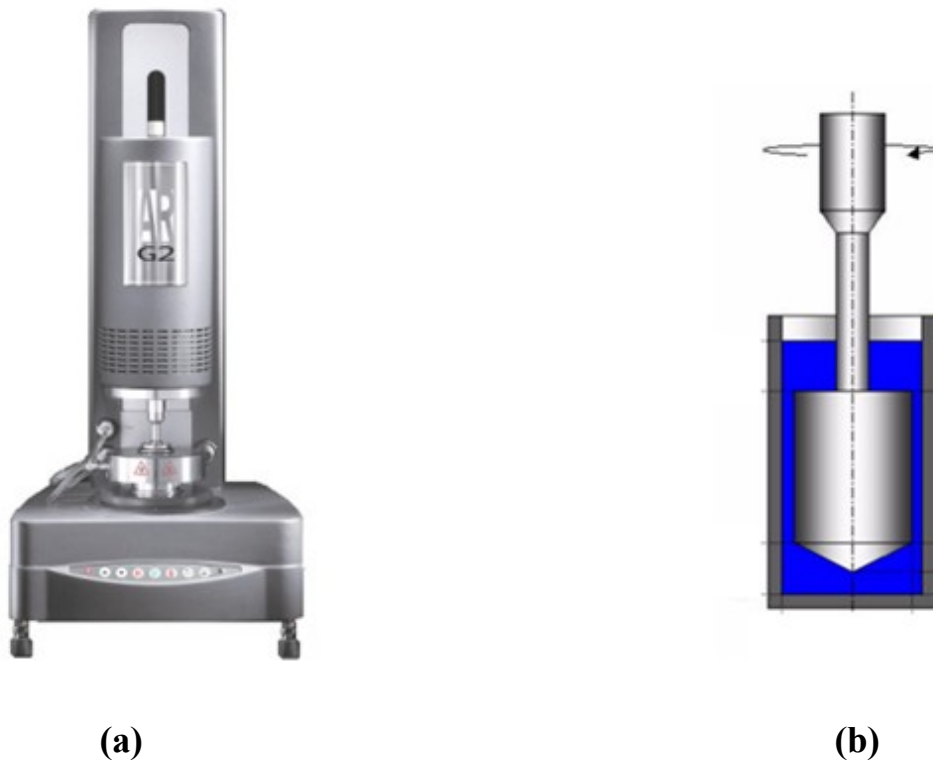


Figure 2.3. (a) Rheometer and (b) Concentric cylinder geometry.

2.3. RESULTS AND DISCUSSION

2.3.1. Viscosity of Aged Diluted Bitumen Solutions

Bitumen Diluted in Heptol (80:20)

We followed the changes of the viscosity of bitumen dissolved in heptol (80:20) over period of 30 days for three different concentrations 5, 11, and 40 wt.%. For each concentration six solutions were prepared and aged for different times. The measured samples were taken from the supernatant of unperturbed solutions. Figure 2.4 shows the variation of viscosity of bitumen as a function of time. The viscosity of 40 wt.% bitumen sample did not change in time. The viscosity of 5 and 11 wt.% almost reached a plateau after 8 days and it decreased of about 12 % after 30 days.

We did not observe formation of precipitates for 40 wt.% solutions and apparent sediment was formed at the bottom of vials for 5 and 11 wt.% solutions. This observation agrees with previously reported value for critical S/B ratio in case of heptol (80:20) S/B ratio.^{11, 12, 20, 67} As the initial precipitates formed in the solution at bitumen concentrations of 5 and 11 wt.% were initially removed out by centrifugation as described in Materials section, the results in Figure 2.4 support the notion that above the critical S/B the aggregation of asphaltenes and formation of precipitates which can settle is a continuous process in agreement with Long et al.⁶⁸ who also reported continuous process of asphaltenes aggregation. The secondary asphaltenes precipitation continues for days.²⁰

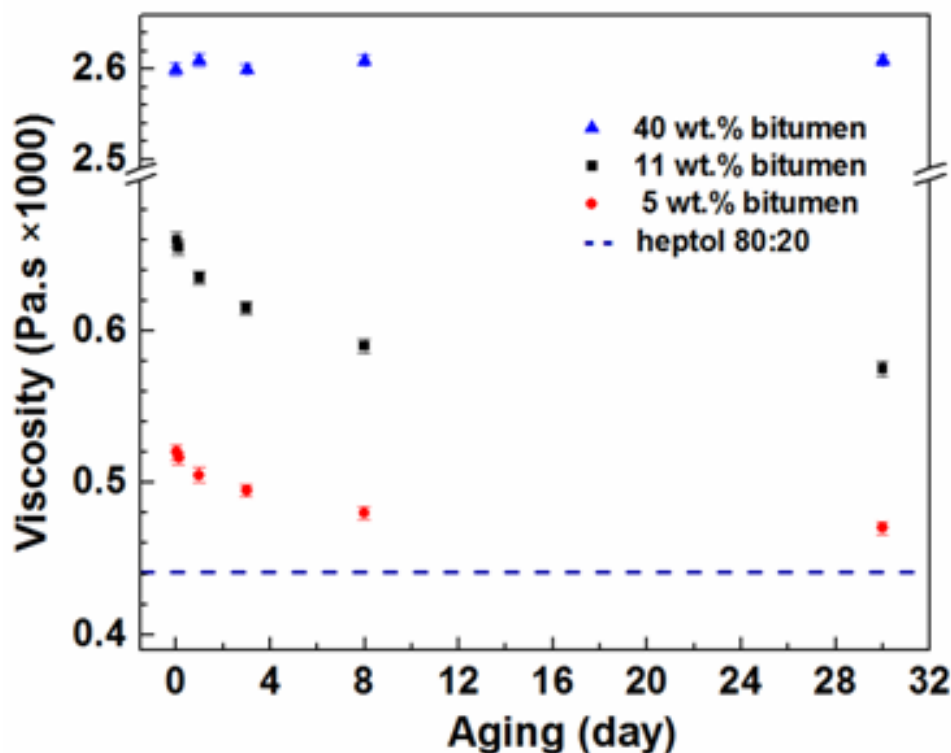


Figure 2.4. Viscosity of bitumen diluted in heptol (80:20) as a function of aging time. The errors in viscosity measurements are less than 0.008 mPa·s.

Viscosity of Bitumen in Heptane

Viscosity change with aging for bitumen dissolved in heptane solutions is shown in Figure 2.5. Similarly to the heptol (80:20) case, for the concentrations above critical S/B ratio, 5 and 11 wt.%, the viscosity of the supernatant decreased significantly in time, ~ 9 % drop after 30 days. The decrease of the viscosity is most likely related to the precipitations of asphaltenes and their settling at the bottom of the vial.

Another possibility could be that even though the asphaltene aggregates stay dispersed in the solution, they become more compact and their effective volume in the solution decreases, which reduces the solution viscosity.

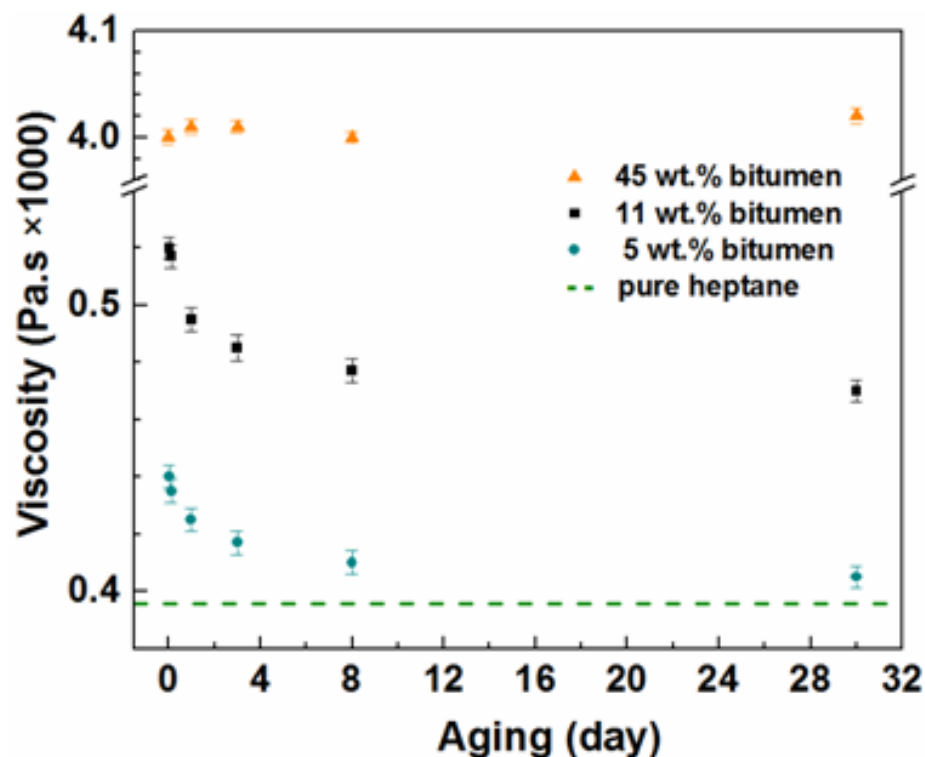


Figure 2.5. Viscosity of bitumen diluted in heptane as a function of aging time.

The errors in viscosity measurements are less than 0.008 mPa·s.

Viscosity of Bitumen in Toluene

The viscosity of bitumen diluted in toluene did not change with time. The viscosity of 11 wt.% bitumen in toluene solution was constant at $\eta = 0.85 \text{ mPa} \cdot \text{s}$ for up to 30 days. The experimental errors in viscosity measurements were determined to be less than 0.008 mPa·s. Centrifugation at 16,000 g for 60 min of aged solutions of bitumen in toluene did not change the viscosity of the solution, which confirms the absence of precipitates and large aggregates in these solutions.

The viscosity measurements of diluted bitumen solutions in time showed two different trends: (1) viscosity of bitumen diluted in heptane and in heptol (80:20)

above the critical S/B ratio decreased with aging; (2) viscosity of solutions of bitumen in heptane and in heptol (80:20) below the critical S/B ratio and in toluene did not change with aging.

2.3.2. Bitumen Content of Supernatant of Aged Solutions

One possible explanation of the results in the previous section is that even after the initial precipitates were removed (all solutions were left to rest for one day after preparation and then centrifuged before being aged for prolonged periods) the process of aggregation continues and leads to formation of large aggregates that settle out of the solutions. Then the supernatant of the solution becomes depleted of asphaltenes and consequently the measured viscosity is reduced. To check this hypothesis we have measured the bitumen content of supernatants for solutions above the critical S/B after different aging times. The result show that the bitumen content in the bulk of the solutions decreases with aging time, see Figure 2.6. After 30 days of aging the bitumen content decreased of about 29% in heptol (80:20) and 35% in heptane. The initial asphaltenes concentration in heptane is about 14 g/L and the estimated asphaltenes content after 1 and 8 days reaches to 2.6 and 0.8 g/L, respectively. The decreased bitumen content indicates the formation of large aggregates in the solution that settle down and as a results the measured viscosity is reduced. Above the critical S/B, initially we observed a fast precipitation, which takes place for a less than one hour, followed by a slow precipitation process with the time scale of several days.

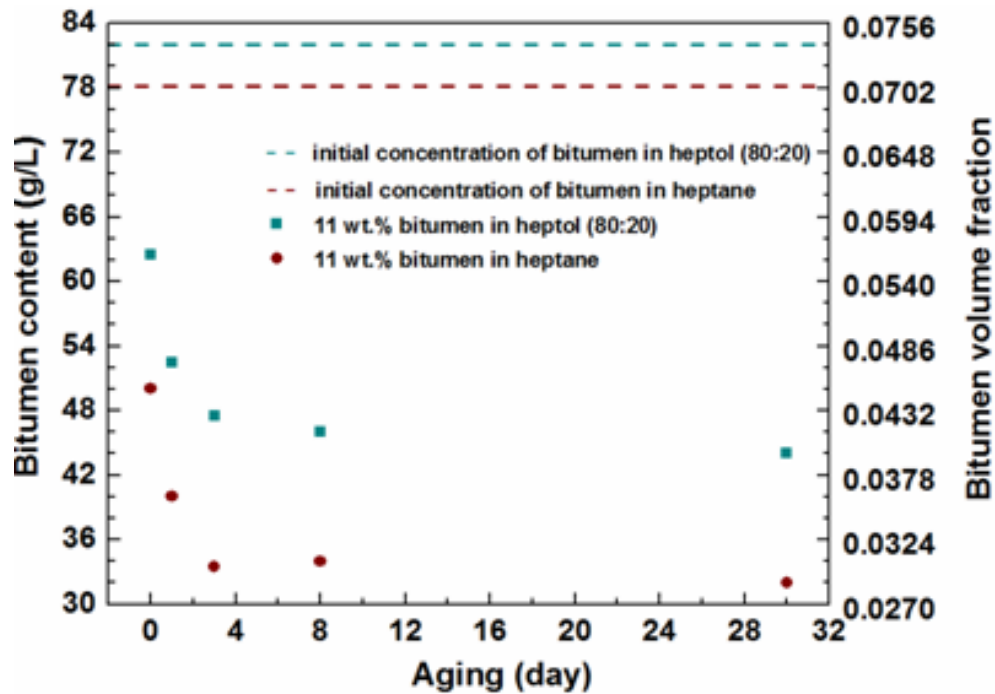


Figure 2.6. The bitumen content and volume fraction of 11 wt.% bitumen diluted in heptol (80:20) and heptane as a function of aging time.

2.3.3. Newtonian Behavior of Bitumen Solutions

As we mentioned in the Introduction, it was suggested recently that asphaltene aggregation is the reason for non-Newtonian drainage of thin liquid film (separating two water phases) for bitumen in heptol and in heptane solutions at concentrations above the critical S/B ratio.^{11, 12, 20, 67} Such non-Newtonian behavior of the film liquid was proposed to be a new mechanism for stabilization of water in oil emulsions.

The experiments that showed such non-Newtonian behavior were performed for a similar system and concentrations as the system studied in this work. However, this previous work was for thin liquid films, where the oil drains at confined geometry between two water/oil interfaces in close proximity of less than

100 nm. We tried to examine a possible non-Newtonian rheology in the bulk of our solutions by measuring the shear stress versus shear rate. As illustrated in Figure 2.7 and Figure 2.8, the y-axis and x-axis represent the shear stress and shear rate of 5 wt.% bitumen in heptol (80:20) and heptane, respectively. The graphs clearly show that the intercept is very close to the zero. We also plotted the results for 11 wt.% bitumen in toluene, heptane and heptol (80:20) that is shown in Figure 2.9. We found a linear dependence with well-defined slope for different solvents, which corresponds to Newtonian liquids of different viscosities. The Newtonian character of bulk solution of bitumen is not a surprise and agrees with previous works.^{16, 17, 64} It looks like non-Newtonian behavior is important in small gaps and in presence of water/oil interfaces.

The confirmation of possible non-Newtonian behavior in bulk solutions probably will require more sensitive methods capable of detecting the small values of the reported yield stress.^{11, 67}

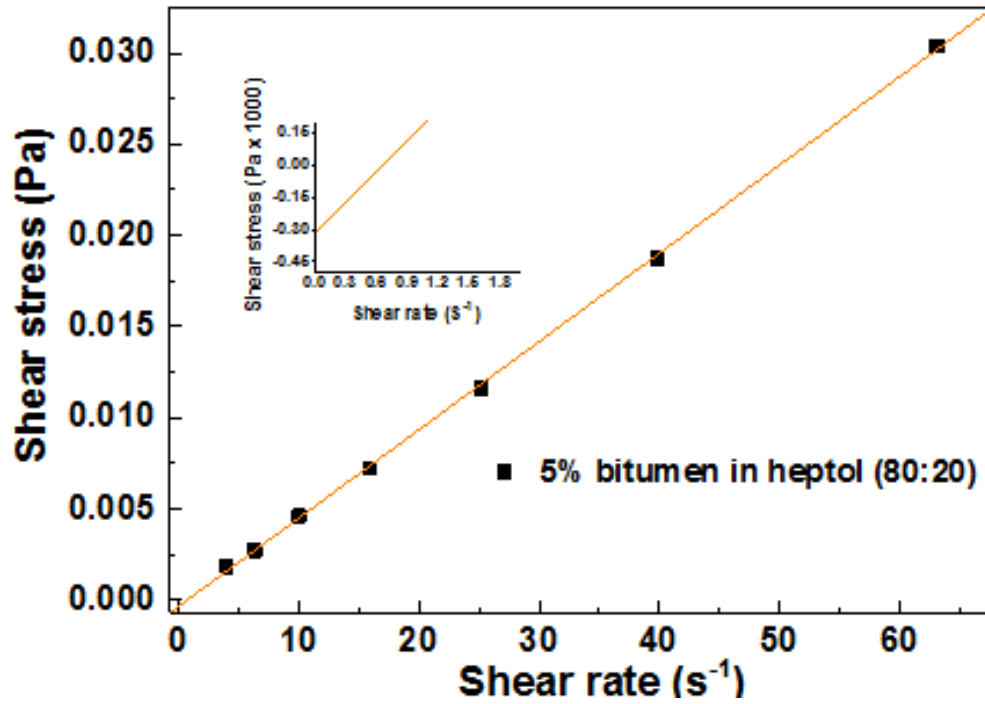


Figure 2.7. Shear stress versus shear rate for 5 wt.% bitumen in heptol (80:20).

Sample was centrifuged at 16,000 g for 60 min with 7 days aging time.

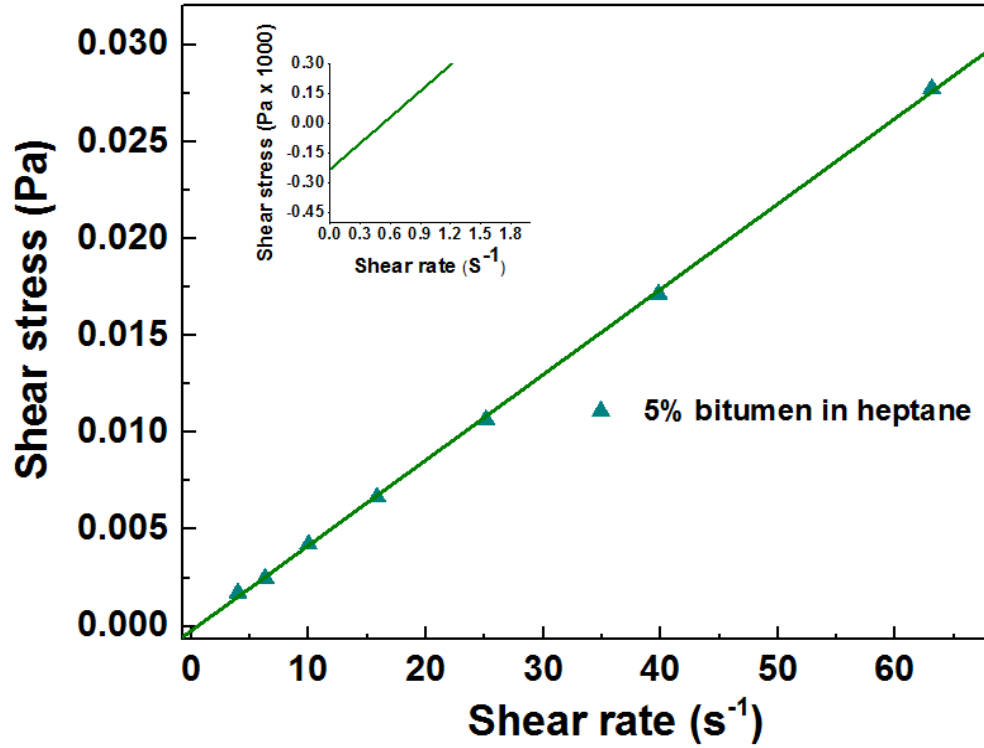


Figure 2.8. Shear stress versus shear rate for 5 wt.% bitumen in heptane. Sample was centrifuged at 16,000 g for 60 min with 7 days aging time.

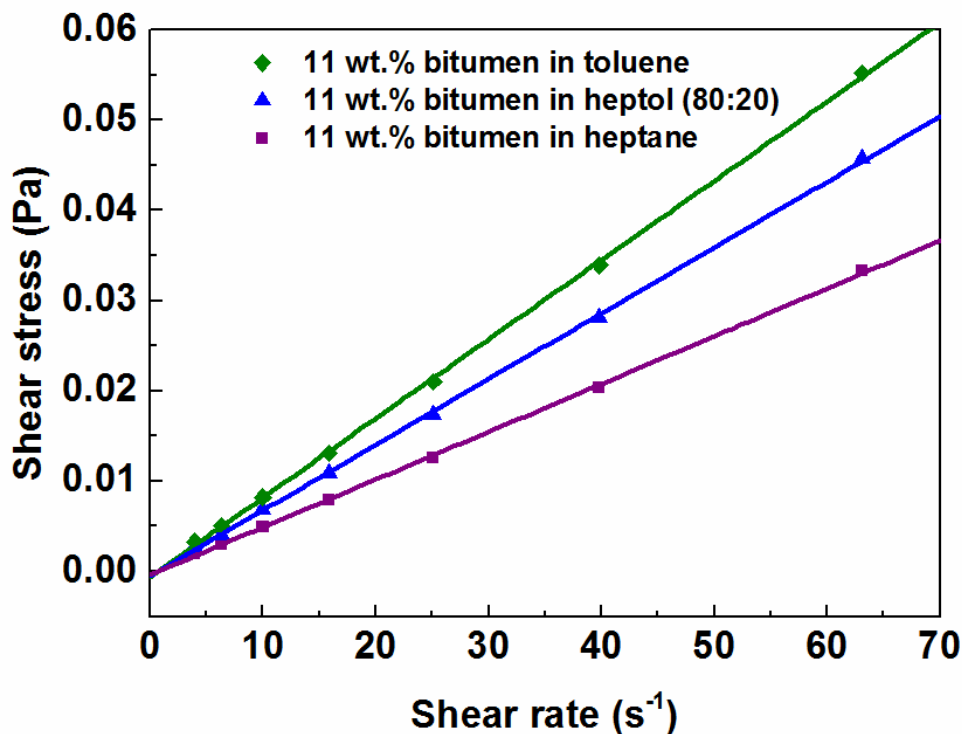


Figure 2.9. Shear stress versus shear rate for 11 wt.% bitumen in different solvents. Samples were centrifuged at 16,000 g for 60 min with 0 day aging time.

2.4. Theoretical Section

2.4.1. Effective Volume Fraction of Dispersed Bitumen and Asphaltenes

The evolution of asphaltenes aggregation from the molecular to the cluster state was first presented by Yen et al.⁶⁹ They investigate the structure of asphaltenes by using X-Ray Diffraction (XRD) technique. Asphaltenes have been studied extensively based on colloidal approach. Numerous efforts have been made to define a solid model to evaluate the viscosity of asphaltenes solution, however; this issue is still unresolved.⁷⁰ Prediction of heavy crude oil and bitumen viscosity based on asphaltenes content is very important since asphaltenes content significantly influence the viscosity unlike other fractions of bitumen.

Several empirical and semi-empirical viscosity modeling have been proposed but it seems that these models still cannot describe every asphaltene systems.⁷⁰

In these sections we intend to analyze the viscosity results in terms of colloidal suspension models. The relationship between the relative viscosity η_r (ratio of solution viscosity to the dispersing liquid viscosity) and the volume fraction of dispersed phase ϕ (hard spherical particles) can be expressed as^{71, 72}

$$\eta_r = 1 + k_0\phi + k_1\phi^2 \quad (1)$$

where k_0 and k_1 account for the Einstein and Huggins constants, respectively.

The viscosity of suspension of non-interacting spherical particles can be presented with the Einstein equation:

$$\eta_r = 1 + 2.5\phi \quad (2)$$

This equation is valid in a diluted regime, where $\phi < 0.15$.⁷³

For hard spheres of different sizes, Roscoe⁷⁴ proposed the following relation of relative viscosity as a function of volume fraction.

$$\eta_r = (1 - \phi)^{\frac{5}{2}} \quad (3)$$

This equation reduces to the equation (2) in high dilution regime.

Pal and Rhodes⁷⁵ developed a semi-empirical model using the effective medium approach to express the following model:

$$\eta_r = (1 - K' \phi)^{\frac{5}{2}} \quad (4)$$

where K' is the solvation coefficient. This coefficient is considered to be the effect of solvent (i.e. continuous phase) immobilization at the particles surface.⁷⁰

Therefore, when particles are solvated they have larger volume in comparison with their dry state. If we plot the $\eta_r^{-\frac{2}{5}}$ as a function of ϕ then expect a straight line with a slope of $-K'$ and an intercept of 1.

Krieger⁷⁶ proposed the popular semi-empirical model in which the effect of particles jamming is also taken into the consideration. The model is presented as

$$\eta_r = \left(1 - \frac{\phi}{\phi_{\max}}\right)^{-\frac{5}{2}} \quad (5)$$

where ϕ_{\max} is defined as the maximum volume fraction packing of particles.

If we consider bitumen or asphaltenes as colloidal dispersions of spherical particles in the solution, the equation (2) and (3) can be used to estimate the volume fraction of bitumen/asphaltenes.

2.4.2. Effective Volume Fraction of Dispersed Bitumen

Roscoe model was used to estimate the volume fraction of dispersed bitumen since Einstein model is limited to dilute regime. The change of effective volume with aging time is compared for 11 wt.% bitumen in different solvents. As illustrated in Figure 2.10, the effective volume of bitumen in toluene is nearly constant while those of heptol (80:20) and heptane are decreasing with aging. The decrease in the initial values of effective volume fraction of bitumen in heptol (80:20) and heptane is related to the precipitation and rejection of some of the asphaltenes during the centrifugation of initial solutions.

Both, the Roscoe and Einstein models were used for estimation of effective volumes of 11 wt.% bitumen in heptane. Results based on the two models converge at lower bitumen volume fraction, as expected. The difference in the

estimated bitumen volume fraction can be explained with the fact that Roscoe model accounts for spherical particles which vary greatly in size and hydrodynamic interactions between the particles are taken into the consideration, unlike in the Einstein model.

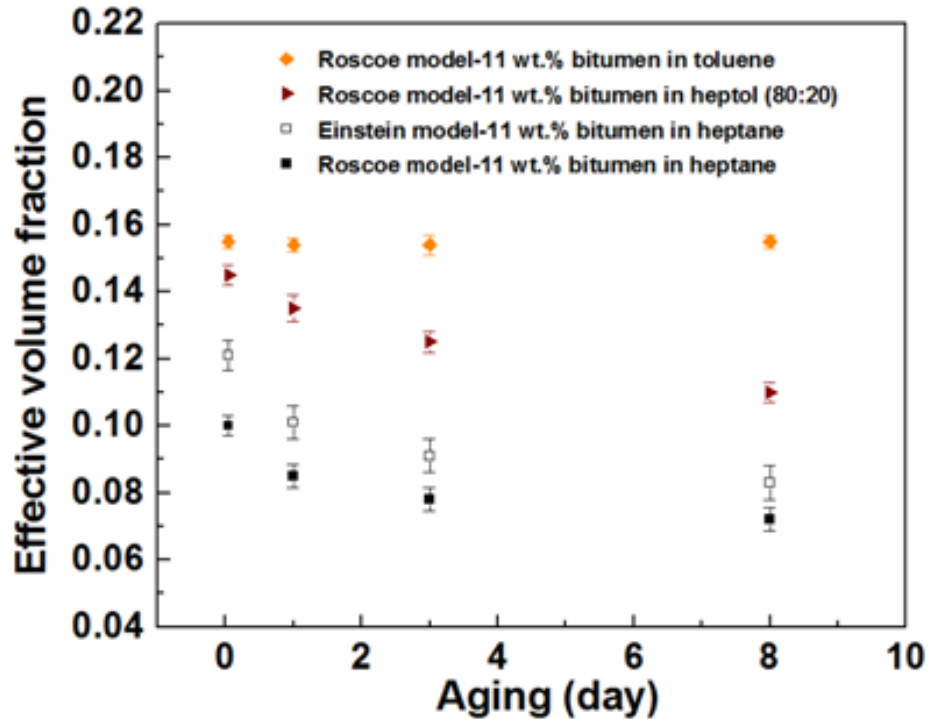


Figure 2.10. Effective volume fraction of bitumen in different solvents as a function of aging. The errors in the estimated volume fraction are less than 0.006.

2.4.3. Volume Fraction of Dispersed Asphaltenes

The viscosity of bitumen is determined mainly by the asphaltenes subfraction.¹² If we assume the deasphalted bitumen to be the continuous phase and consider it as a medium for the dispersed asphaltenes, the relative viscosity can be defined as a ratio of the viscosity of aged bitumen solution to the viscosity of the

deasphalted bitumen solution. We considered 30 days aged 5 and 11 wt.% bitumen solutions to represent deasphalted bitumen as no noticeable asphaltene precipitation occurred after further dilution with heptane. The volume fraction of dispersed asphaltene for different aging times can be estimated again using equations (2) and (3). The effective volume fractions of asphaltene versus aging time are shown in Figure 2.11 and Figure 2.12. The difference in the volume fraction of asphaltene in heptol (80:20) and heptane with the same bitumen concentration can be explained by lower solubility of asphaltene in heptane than in heptol (80:20) and different rates of asphaltene aggregation and precipitation in these solvents.

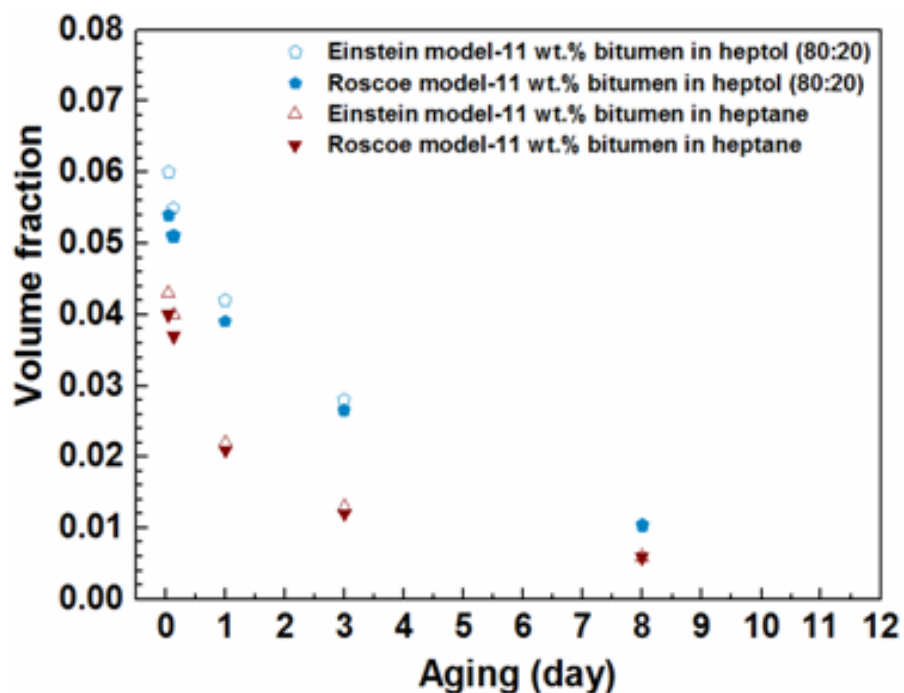


Figure 2.11. Volume fraction of asphaltene as a function of aging in bitumen solutions. The errors in the estimated volume fraction are less than 0.008.

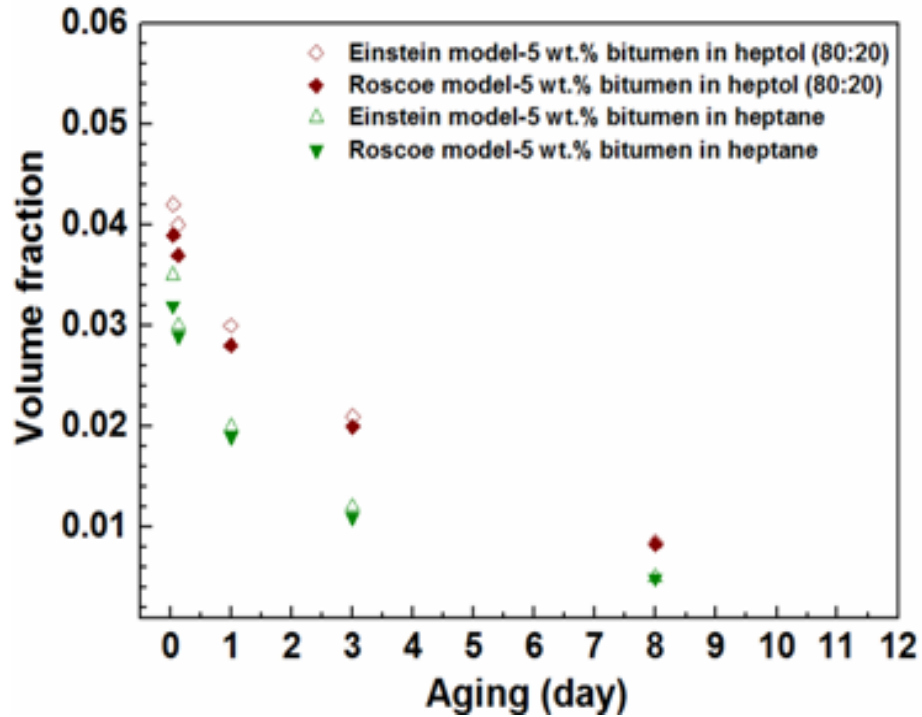


Figure 2.12. Volume fraction of asphaltenes as a function of aging in bitumen solutions. The errors in the estimated volume fraction are less than 0.009.

2.5. CONCLUSION

Asphaltenes initially form small nano-aggregates and then evolve into nano-aggregate clusters which eventually form larger particles and precipitate. According to our results, it is telling to state that aging the bitumen solution above the critical dilution accounts for reduction in the viscosity. This phenomenon can be addressed to the incessant asphaltene aggregation and precipitation resulting in their removal from the bulk phase. On the other hand, removal of small nano-aggregates by centrifugation led to a small decrease in the volume fraction of dispersed bitumen which cannot induce significant effect on the viscosity. The observed time dependence of the viscosity reduction suggests

that the asphaltenes aggregation/precipitation is a continuous process with the time scale of weeks. Newtonian fluid behavior was observed for bitumen solutions at room temperature for different solvents regardless of critical S/B ratio. Viscosity modeling shows that the effective volume fraction of bitumen in toluene is larger compared to heptol (80:20) and heptane. The reduction in volume fraction of bitumen based on viscosity modeling agrees with the experimental values. Moreover, by comparing the volume fraction of bitumen and asphaltenes in heptane and heptol (80:20), the lower value is observed for heptane. This observation corresponds to the insolubility of asphaltenes and higher precipitation rate in heptane. These results add to current understanding of the relation between aggregation of asphaltenes and viscosity of diluted bitumen, which is important for improving heavy oil extraction and processing technologies.

Chapter 3. Nanofluidic Devices for Rheology Analysis of Diluted Bitumen

3.1. INTRODUCTION

Nanofluidics is defined as the study of fluid flow in spaces with at least one critical dimension below 100 nm.³⁰ In the recent decades, nanofluidic devices have found wide range of applications in rheological analysis⁷⁷, molecular separation⁷⁸, drug delivery⁷⁹ and desalination³³. In addition, very low sample is needed in nanofluidic platform which provides great opportunity to study the biological system, such as single cell.³² Nanofluidic devices acquire extremely high surface area to volume ratio, therefore, surface-liquid interactions become extensively important.⁸⁰

Due to immense interest in this area, disposable devices and low cost fabrication methods are highly attractive for many research institutes.³⁶ Various materials including silicon, glass, polydimethylsiloxane (PDMS) and polymethylmethacrylate (PMMA) are currently used to fabricate nanofluidic devices for specific applications.³¹ Nanofluidic devices made out of glass have the advantages of optical transparency, electrical isolation and high mechanical strength.⁸¹ Moreover, Glass chips have good compatibility with organic solvents, such as, heptane, toluene, and pentane. Glass-glass bonding is a crucial step in the fabrication steps.

A version of this chapter has been submitted to the journal of Microfluidics and Nanofluidics and is under review for publication.

Thermal fusion bonding at high temperature enhances the bonding strength, however, channels distortion and collapse can happen for a long time process of bonding at high temperature.⁸² Successful and effective glass-glass bonding depends on the surfaces cleanness and flatness, channels aspect ratio, bonding temperature and applied pressure.^{81, 82}

Nanofluidic devices can also be fabricated with different aspect ratios (AR) for the variety of applications. AR is defined as the ratio of channel height to width. Kuo et.al⁸³ reported the fabrication of nanochannels in glass with the depth of 20 nm and aspect ratio of 0.001 using thermal fusion bonding. Pinti et.al⁸⁴ fabricated ultra-low AR (i.e., $w \gg h$) nanochannels as shallow as 16 nm in borosilicate glass using PDMS adhesive bonding. Ultra-low AR nanochannels can provide higher volumetric flow for the same pressure drop in comparison to the channels which acquire nanometer scale in two dimensions.³⁸

Ultra-low AR nanochannels facilitate the flow analysis as the flow can be easily traced via optical microscope. Pressure-driven and electro-osmotic flows (EOF) are the main methods of fluid transport in micro-nanofluidic devices. EOF systems are the preferred methods where the separation of mixture is desired.⁴¹ However, their applications are limited to the aqueous solutions.⁴² Unlike in EOF, Pressure-driven flows can be used for any type of solvents. Therefore, pressure-driven flows receive great attention when using organic solvents.⁴²

In the nanofluidic devices, large pressure drop is expected due to the extremely small hydraulic diameter of system. Thus, high pressure up to MPa and very low flow rate are necessary to generate the flow and avoid nanofluidic chip damage.

Fluids at the nanoscale exhibit different properties from those observed in the bulk. Hibara et al.⁸⁵ investigated aqueous solutions properties in the nano-confinement geometry by time-resolved fluorescence spectroscopy. They found that the solutions have larger viscosity in the nanochannels in comparison with their bulk values. In their point of view, the interaction between the channel wall and hydrogen bond network might be the reason for increase in the viscosity. Tamaki et.al⁴² developed a nanofluidic platform to control the flow in the nanochannels. They observed the viscosity of aqueous solution at the nanoscale is larger than that of measured in the bulk which was attributed to the effect of size confinement on solution viscosity.

Large surface area to volume ratio is the characteristic of nanofluidic systems; therefore, capillary action is found to be very important.⁴⁴ Capillary action is the result of adhesion force between liquid-wall and air-liquid surface tension that leads to spontaneous filling of nanochannels.⁴⁵ Wall surface properties play a key role in the filling kinetics of liquids in the nanochannel.⁴⁵ However, the way liquid wets the nanoscale surface is not fully understood.⁸⁶

In the nanoscale channels van der Waals forces also become important and their interplay with surface tension forces changes liquid wetting properties.^{87, 88} Liquid surface tension, dynamic contact angle, channel hydraulic diameter, liquid nature (i.e. Newtonian or non-Newtonian) and its viscosity are the main parameters in determining liquid filling kinetics.

As shown in several studies, penetration velocity of capillary flows in the nanoscale differs from the theoretical predictions.^{43, 44, 47, 89} Tas et al.⁴⁴

investigated the capillary filling of water in 100 nm deep channel and they found the filling speed of water is lower than the expected values achieved by theory. This observation was addressed to the electro-viscous effect. Kuo et al.⁴⁵ compared the experimental filling velocity of water in the nanochannels with numerical and theoretical results. They found that filling velocity in the experimental results is in good agreement with the numerical analysis but lower than the predicted values based on Washburn⁴⁶ model.

Several studies demonstrated that the liquid filling speed decreases as the nanochannel size reduces.^{43, 45} Kim et al.⁴³ studied the wetting properties of non-polar prepolymer liquid inside nanofluidic system. Multi-curvature meniscus was observed at the front of advancing liquid which attributed to the presence of intermolecular interactions near to the nanochannel wall. Rossi et al.⁸⁶ by using environmental scanning electron microscopy (ESEM) showed that water confinement inside carbon nanotubes and its interaction with the wall are responsible for the formation of complex meniscus shapes.

Despite numerous researches on rheology of various liquids in the micro-nanoscale, there are few studies on the heavy oil and bitumen flow in such small scale.^{28, 90-92} Bitumen acquires an intricate structure which is categorized in to the SARA classification (i.e. saturates, aromatics, resins, and asphaltenes).⁹³ Asphaltene is a fraction of bitumen composed of various molecules.² Asphaltene is soluble in toluene but insoluble in alkanes such as pentane or heptane.⁵⁶ Moreover, asphaltene is a determining factor in high viscosity of bitumen.^{12, 57, 58}

To decrease the density and viscosity of bitumen during the process of bitumen recovery from oil sands, addition of light hydrocarbon solvent is of a great importance. Furthermore, at the critical solvent to bitumen ratio (S/B), asphaltene starts to aggregate.²⁰⁻²²

Various studies have been conducted to study the role of asphaltenes in the stability of water-in-crude oil (W/CO) emulsions.^{1, 11, 21, 65-67} Bouriat et al.⁹⁴ by conducting interfacial rheology pointed out that asphaltenes form a 2-D network at the water in oil (W/O) interface. Spiecker et al.²⁴ explained that the asphaltenic film formed at the W/O interface shows a viscoelastic behavior. Recently, Czarnecki et al.^{11, 67} and Tchoukov et al.¹² by applying thin liquid film technique demonstrated that asphaltenes form 3-D structure at the W/O interface that alter the rheology of thin oil film from Newtonian to non-Newtonian with small yield stress at the thickness of between 50– 100 nm.

This study aims towards characterizing of oil film rheology below and above critical S/B ratio in a length scale comparable to the film thickness where oil film rheology changes as proposed by Czarnecki et al.^{11, 67} Nanofluidic device provides a great opportunity to measure the rheology of oil film in the nanoscale length which is not possible using conventional rheometer. Using nanofabrication technology, nanofluidic devices will be developed which allows the simultaneous measurements of fluid velocity and viscosity.

3.2. EXPERIMENTAL SECTION

3.2.1. Nanofabrication

Square borofloat glass substrates with the thickness of 1.1 mm were initially cleaned in piranha solution (96% H₂SO₄ and 30% H₂O₂ with the volume ratio of 3:1) for 15 min to remove organics and metallic contaminants. Substrates were placed into the dump rinser to clean the substrates from piranha solution using de-ionized water and then dried in the Spin Rinse Dryer. A positive photoresist (HPR 504) was spun on the substrates and soft-baked at 115 °C for 30 min in Despatch/Blue M oven. Standard UV lithography was applied to pattern the nanochannels, and then the photoresist was developed in 354 developer to remove the exposed areas. After developing the photoresist, nanochannels with rectangular cross-sections were etched into the glass substrates by reactive ion etching (Trion RIE). The etching rate was determined to be 33 nm/min. The etching depth as a function of time is plotted in Figure 3.1. After the etching was finished, photoresist removal was eased with 30 min ultrasonication in acetone. Atomic force microscopy (Dimension Edge, BRUKER) was used to measure the etched surface profile. Schematic of nanofabrication and surface profile measurements are shown in Figure 3.2 and Figure 3.3, respectively. Then, holes were drilled through the unpatterned substrates. In addition, the etched and unpatterned substrates were cleaned in the piranha solution for 15 min, and pressed together to form a temporary bonding.

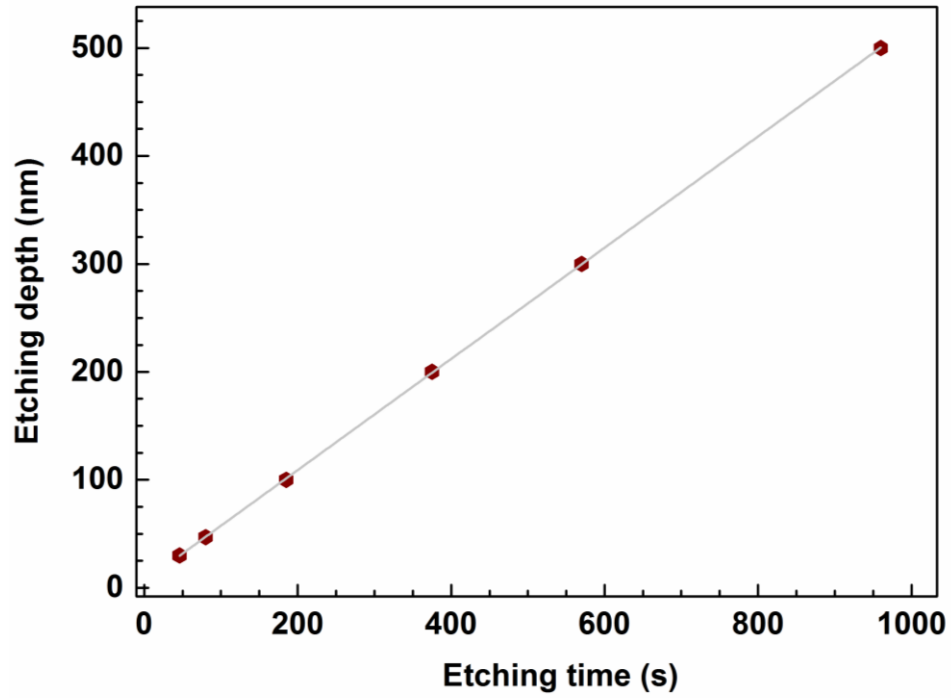


Figure 3.1. Etching depth as a function of etching time using reactive ion etching (RIE).

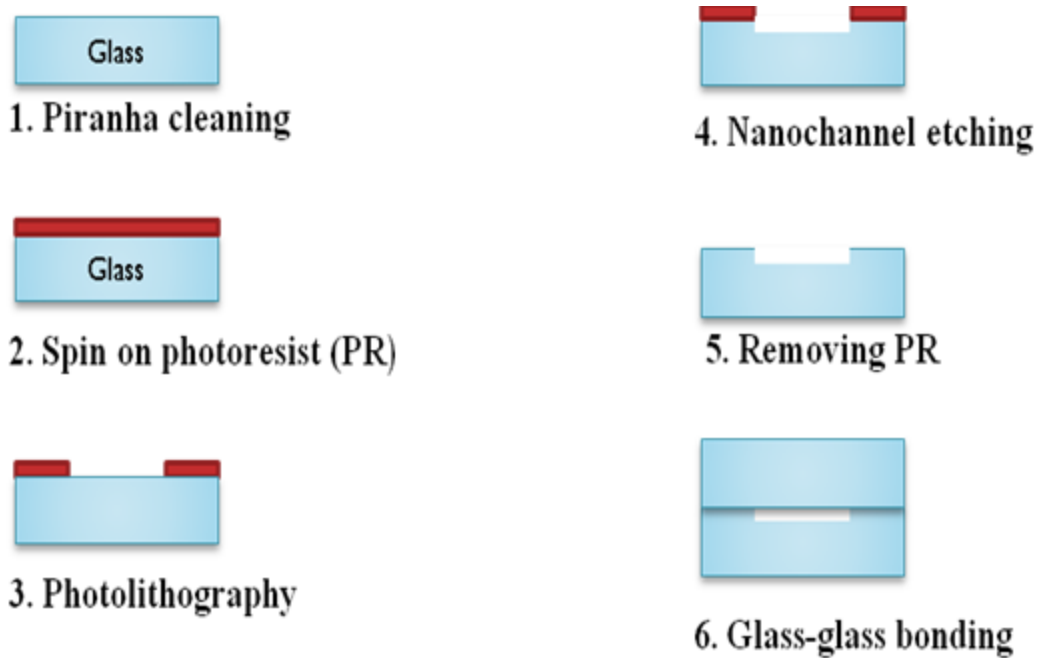


Figure 3.2. Schematic of nanochannels fabrication

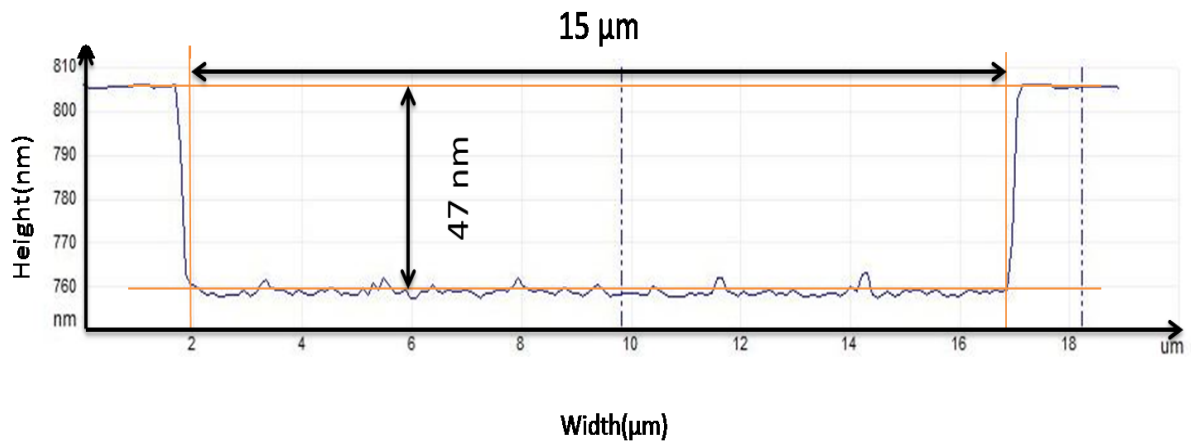


Figure 3.3. AFM image of centimeter long, 15 μm wide, and 47 nm deep channel etched by RIE. The mean roughness (R_a) was determined to be 0.6 nm.

3.2.2. Materials

In this study, Athabasca bitumen was provided by Syncrude Canada Ltd. The bitumen was further diluted with different solvents, such as n-heptane (HPLC grade Fisher Scientific) and heptol (80:20) that is a mixture of heptane and toluene with the volume parentage of 80:20. Heptol (80:20) was used as its solubility properties is close to the naphtha; an industrial solvent mainly used for froth treatment.

3.2.3. Bitumen Samples Preparation and Procedure

50 wt.% bitumen in heptol (80:20) was used to prepare various concentrations of 5, 11, 20, and 40 wt.% diluted bitumen. In all concentrations asphaltenes aggregation/precipitation occurs except for 40 wt.% bitumen that is below critical S/B ratio. Samples were aged for one day to allow the most of solid

particles (i.e. mostly asphaltenes) to settle down. Afterward, supernatants of diluted bitumen were collected and centrifuged at 16,500 g for 30 min at the room temperature to enhance removal of small precipitates. To examine the effect of centrifugation on removal of small aggregates and how removal of small aggregates affect the filling process of bitumen, we prepared 5 wt.% bitumen in heptol (80:20) solutions, which first aged for 1 day and centrifuged at 16,500 g for 30 min and 90 min. Different centrifugation time did not exhibit any noticeable effect on the filling kinetics of bitumen solutions. The Capillary filling process for all solutions was also repeated three times.

3.2.4. Viscosity Measurements

Rheometer ARG2 (TA Instrument) was selected to carry out viscosity measurements. The rheometer was equipped with a temperature control to accurately record the data in the specified temperature. Concentric cylinder geometry was used as it is suitable for low viscosity measurements. The operating gap was set to 5.9 mm as suggested by user manual. However, changing the gap had negligible effect on the measured viscosity. Shear rate was ranged from 1 to 100 s^{-1} . The Experiments were repeated several times and carried out at the 23 ± 0.02 °C. For the calibration purposes, several pure solvents such as water, ethanol (Fisher Scientific), and methanol (Fisher Scientific) were used.

3.2.5. Surface Tension and Bulk Contact Angle Measurements

Surface tension of bitumen solutions diluted in heptol (80:20) and pure solvents were measured at the room temperature using Process Tensiometer (Kruss K-

12). The surface tension data was recorded after 1 min. The contact angle measurement was performed via Theta Optical Tensiometer (T200 Biolin Scientific). The bulk contact angle of various samples was measured on the etched surface of borofloat glass. The etched surface has similar surface properties as the nanochannels that we used in the experiment.

The reported data for surface tension and bulk contact angle as illustrated in the Table 3.1 are the average of three distinct measurements.

3.2.6. Position and Speed of Moving Liquid Meniscus

High speed camera was applied to monitor the position of advancing liquid inside nanochannels. The system was equipped with Labview program to record the data simultaneously.

3.3. THEORY

3.3.1. Newtonian Fluid

Behavior of fluid flow at nanoscale is different from the macroscale one. Flow in microfluidic system dominates by low Reynolds number and exhibits Laminar or Stokes flow.²⁹ It is predicted to be the same for nanofluidic systems.^{29, 95}. For rectangular and ultra-low aspect ratio nanochannel, the nanochannel can be approximated with the parallel plate geometry. The governing equation for solving the Newtonian fluid flow by considering the fact that inertia effect can be neglected is given by:⁹⁶

$$-\frac{\partial P}{\partial x} = -\mu_f \frac{\partial^2 V_x}{\partial y^2} \quad (1)$$

where P , x , μ_f , and V_x correspond to fluid pressure, penetration distance, fluid viscosity and fluid velocity, respectively. In the capillary filling phenomena, the pressure drop is equal to the constant Young-Laplace capillary pressure.⁹⁷ Schematic of capillary-driven flow in a horizontal channel is shown in Figure 3.4.

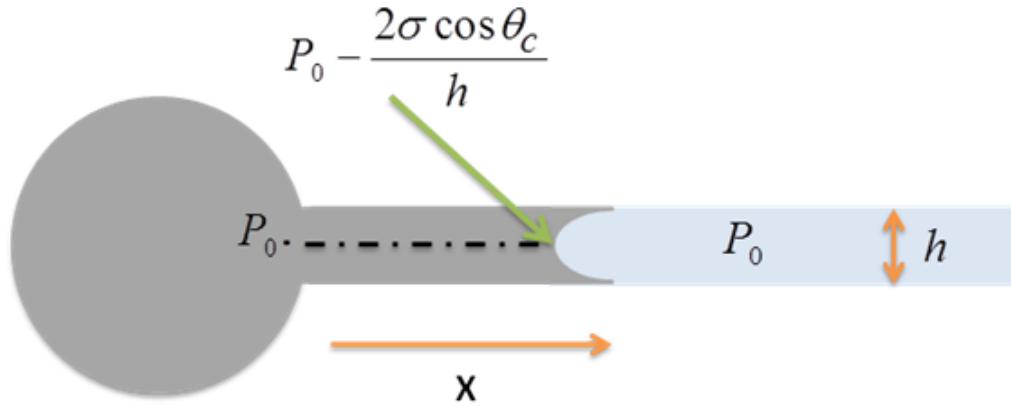


Figure 3.4. Capillary filling of a liquid in the horizontal channel.

The capillary pressure in rectangular and ultra-low aspect ratio channel is shown as follow:

$$\Delta P = \frac{2\sigma \cos \theta_c}{h} \quad (2)$$

By solving equation (1) and combining with equation (2), moreover, assuming quasi-steady state condition, the penetration distance as a function of time and filling speed of advancing liquid can be expressed as^{44, 46}

$$x = \sqrt{\frac{h\sigma \cos \theta_c t}{3\mu_f}} \quad (3)$$

$$V_x = \frac{h\sigma \cos \theta_c}{6\mu_f x} \quad (4)$$

where h is the channel height, σ the air-liquid surface tension, and θ_c the liquid advancing contact angle.

3.3.2. Non-Newtonian Bingham Plastic Fluid

The constitutive equation for Bingham flow in the parallel plate geometry can be demonstrated as

$$\begin{cases} \tau_{yx} = \tau_0 - \mu_B \frac{dV_x}{dy}, & \tau_{yx} > \tau_0 \\ \frac{dV_x}{dy} = 0, & \tau_{yx} < \tau_0, \quad \text{plug flow} \end{cases} \quad (5)$$

where τ_{yx} , τ_0 , and μ_B account for shear stress, Bingham yield stress, and Bingham fluid viscosity. Using the momentum balance the Cauchy stress equation is expressed as

$$-\frac{\partial P}{\partial x} = -\frac{\partial \tau_{yx}}{\partial y} \quad (6)$$

By solving equation (5) and (6), we modified equation (7) solved by Bird et al.⁹⁶ to relate the liquid velocity V_x in the capillary to the penetration distance x :

$$V_x = \frac{\Delta P z^2}{3\mu_B x} \left[1 - \frac{3}{2} \left(\frac{\tau_0 x}{\Delta P z} \right) + \frac{1}{2} \left(\frac{\tau_0 x}{\Delta P z} \right)^3 \right] \quad (7)$$

By substituting equation (2) into equation (7), we get

$$V_x = \frac{\sigma \cos \theta_c z}{3\mu_B x} \left[1 - \frac{3}{2} \left(\frac{\tau_0 x}{\sigma \cos \theta_c} \right) + \frac{1}{2} \left(\frac{\tau_0 x}{\sigma \cos \theta_c} \right)^3 \right] \quad (8)$$

When $\tau_0 = 0$, the equation (8) simplifies to equation (4) for Newtonian Fluid.

Hence $V_x = \frac{dx}{dt}$, the penetration distance as a function time is given by

$$\int \frac{dx}{\left(\frac{\sigma \cos \theta_c z}{3\mu_B} \right) \frac{1}{x} + \left(\frac{z\tau_0^3}{6\mu_B \sigma^2 \cos^2 \theta_c} \right) x^2 - \frac{z}{2\mu_B} \tau_0} = \int dt \quad (9)$$

where $z = \frac{h}{2}$. The equation (9) can be solved numerically using MATLAB software. We applied the trapezoidal rule which is defined in the MATLAB. The spacing was chosen small enough in such a way that the final result would not change significantly.

3.4. RESULTS and DISCUSSION

3.4.1. Capillary-Driven Flow of Pure Liquids

Filling kinetics of pure water, ethanol and methanol have been studied in the ultra-low AR channel with a depth of 47 nm. The liquids were first introduced to the nanochannel via capillary action through the 2 mm holes. To analyze the liquids filling kinetics, high speed camera with a frame rate of 20 images/second was used to simultaneously record the filling process.

In all experiments, geometry parameters of nanochannels, such as depth and width were kept the same. Furthermore, experiments were conducted at the room temperature. The position of advancing liquids as a function of square root of

time for different pure liquids is plotted in Figure 3.5. The graph shows for all liquids the penetration distance linearly changes with a root square of time. This linear dependency is expected for flow of Newtonian fluid. If we assume the contact angle of advancing liquid to be constant and equal to the measured values in the bulk, therefore; equation (3) can be used to calculate the theoretical viscosity in the nanochannel. For methanol and ethanol, the theoretical viscosity is very close to the bulk viscosity measured directly by ARG2 rheometer. For ethanol, the variation of theoretical viscosity as a function of penetration distance was plotted in Figure 3.6. In the case of water, theoretical viscosity seems to be larger. Several researches put a lot of efforts to understand whether the viscosity in the nanoscale is different from the macro one.^{42, 44, 85} Nevertheless, this subject seems to be very challenging. Despite the fact that viscosity of water was reported to be larger in the nanoscale than in the bulk, however; addition of salt to the water could significantly reduce the electroviscous effect.⁴⁴ Therefore, the observed difference in the bulk and nanoscale viscosity became small.⁴⁴

Filling kinetics of both methanol and ethanol is in good agreement with the theoretical predictions. However, as we expected the filling speed of pure water was slower than the calculated value from theory. In order to understand how the liquids deviate from the theoretical predictions, we can rewrite equation (3) as follows:

$$\frac{x}{k} = \sqrt{t} \quad (10)$$

where $k = \sqrt{\frac{h\sigma \cos \theta_c}{3\mu_f}}$. Based on theory, the plot of x/k versus \sqrt{t} should have the slope of unity. By assuming that the advancing contact angle is constant and the viscosity in the nanochannel is equal to the measured value in the bulk, x/k versus \sqrt{t} can be plotted for different liquids. Figure 3.7 shows that the ethanol and methanol follow the theoretical trend quite well. However, water deviates from the theoretical prediction.

In the case of water, we also observed formation of air bubbles. This phenomenon was reported in literature as well.^{44, 47}

As shown in Figure 3.8, the y-axis and x-axis are representatives of advancing liquid velocity and penetration distance, respectively. Equation (4) clearly shows that the velocity decreases as the liquids penetrates further ($V_x \propto \frac{1}{x}$). As time goes by, more liquid will be sucked into the channel. Due to the fact that capillary pressure that pulls the liquid inside is constant, the liquid velocity has to decrease as it penetrates further.

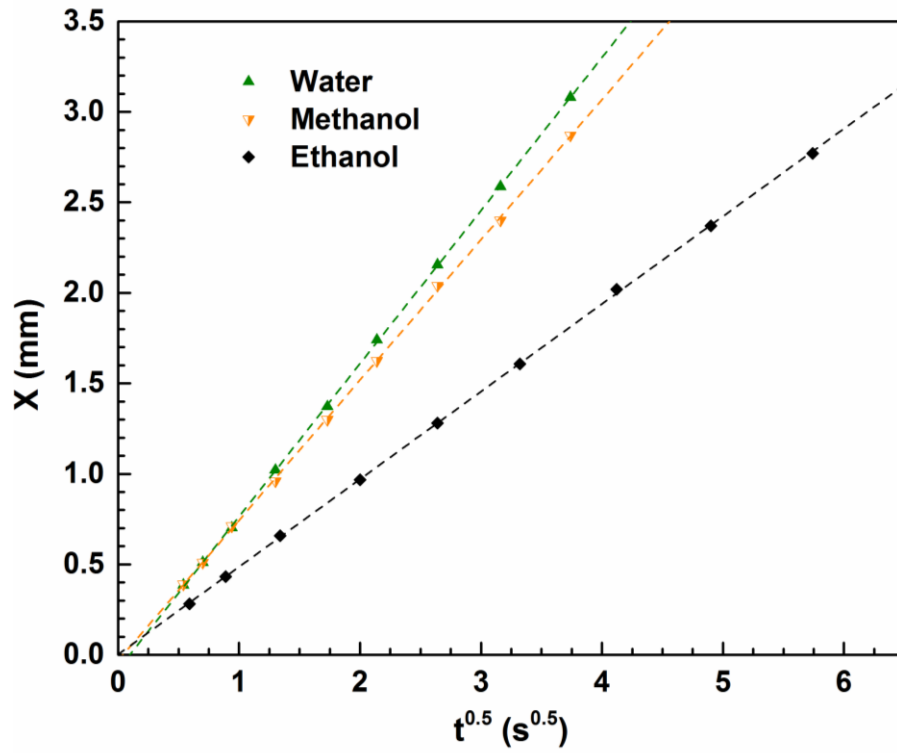


Figure 3.5. The Penetration of pure liquids as a function of $t^{0.5}$ in nanochannel with the depth and width of 47 nm and 15 μm , respectively.

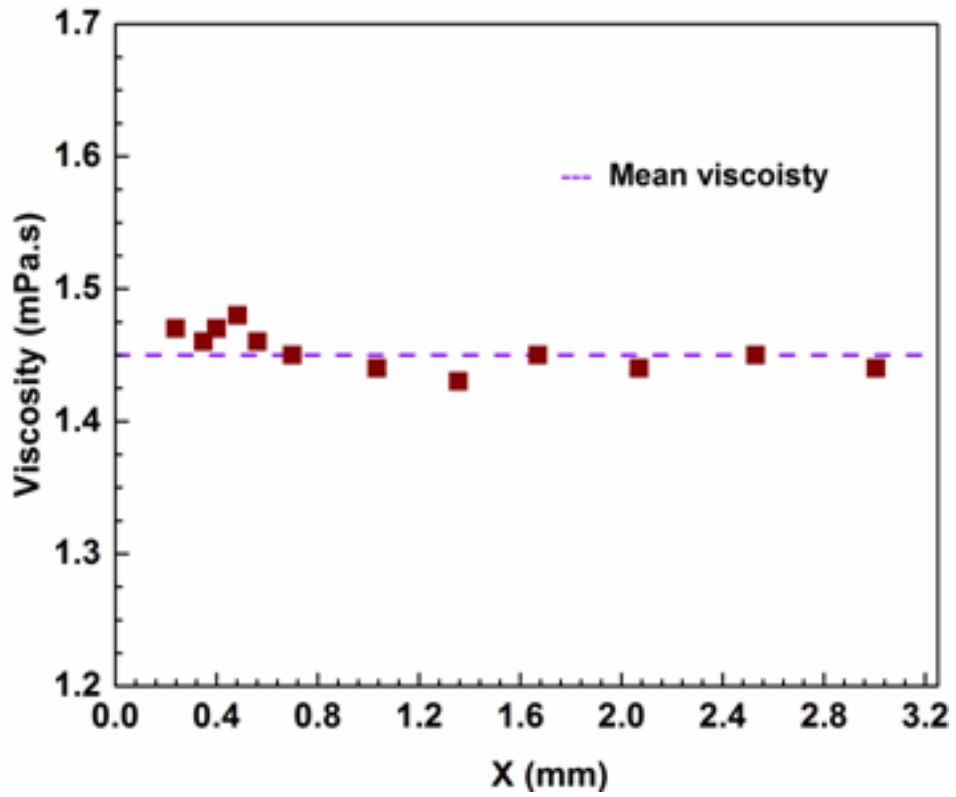


Figure 3.6. The variation of theoretical viscosity for ethanol as a function of penetration distance in nanochannel with the depth and width of 47 nm and 15 μm , respectively.

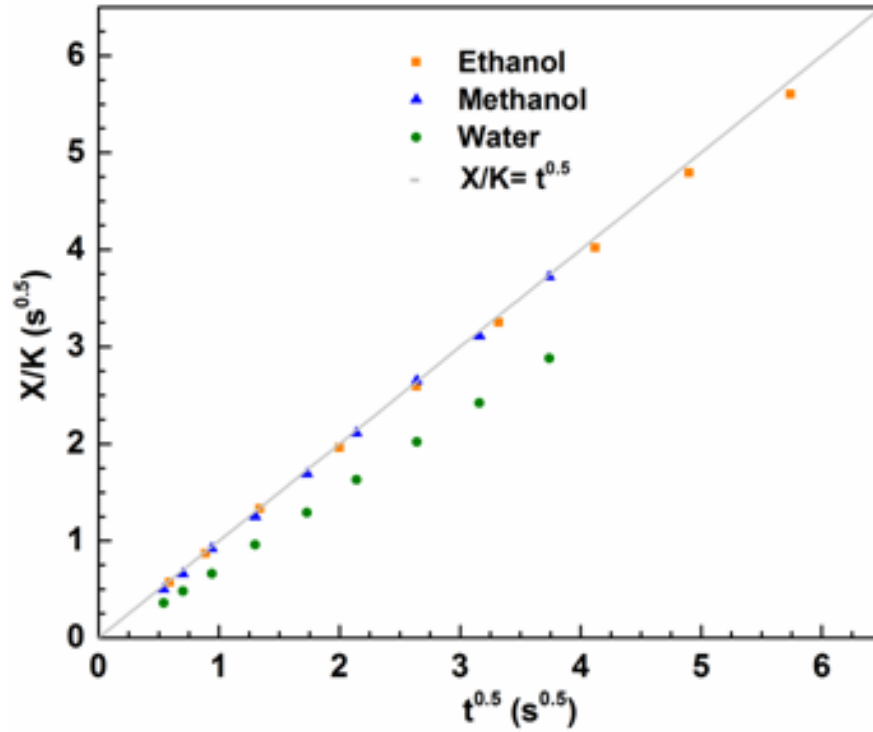


Figure 3.7. The variation of x/k as a function of $t^{0.5}$ for capillary flow of pure liquids in nanochannel with the depth and width of 47 nm and 15 μm , respectively.

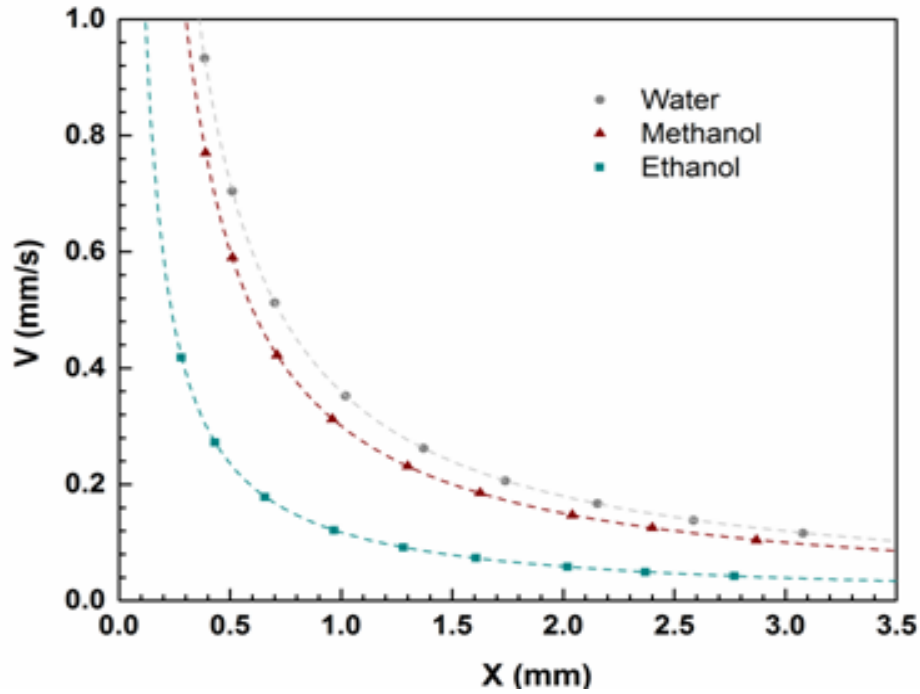


Figure 3.8. The velocity of advancing liquids as a function of penetration distance in nanochannel with the depth and width of 47 nm and 15 μm , respectively.

3.4.2. Capillary-Driven Flow of Bitumen Solutions

To study the filling process of bitumen solutions in the nanofluidic system, bitumen with various concentrations 5-40 wt% were diluted in the heptol (80:20). The position of advancing meniscus as a function of square root of time for bitumen solutions is shown in Figure 3.9. It can be seen from the graph that the position of advancing meniscus changes linearly with square root of time. Figure 3.10 illustrates how bitumen solutions with different concentrations follow the theoretical prediction. By considering the experimental errors, the results for heptol (80:20), 5 and 11wt.% bitumen in heptol (80:20) are

in good agreement with the theoretical result. However, we observed a large deviation as the bitumen concentration increases. In the case of 20 and 40 wt.% bitumen diluted in heptol (80:20), the large variation in the dynamic contact angle of advancing meniscus within the line of wetting was noticed. As shown in Figure 3.11, Figure 3.12, Figure 3.13, and Figure 3.14, the dynamic contact angle of advancing meniscus continuously changes as the 40 wt.% bitumen diluted in heptol (80:20) penetrates further. Therefore, no well-defined contact angle can be observed. We can conclude that assumption of constant contact angle in the case of 20 and 40 wt.% bitumen diluted in heptol (80:20) is totally invalid and in our opinion it is the main reason for the observation of such large deviation. In the studied length scale of bitumen solutions penetration, we also observed formation of air bubbles in the case of 20 wt.% bitumen diluted in heptol (80:20) and is presented in Figure 3.15. Presence of asphaltenes aggregates might be responsible for limiting the liquid flow and leading to formation of air bubbles in the nanochannel.

Advancing meniscus velocity as a function of penetration distance for bitumen solutions is shown in Figure 3.16. After penetration of liquids for distance of about 0.5 mm, the meniscus velocity of 20 and 40 wt.% bitumen diluted in heptol (80:20) drops to 0.13 and 0.04 mm/s, respectively.

Nanochannel blockage repeatedly occurred very fast during capillary filling of 20 wt.% bitumen diluted in heptol (80:20) which is clearly as a result of asphaltenes aggregation/precipitation. However, the nanochannel blockage did not occur for a long time in the case of 40 wt.% bitumen diluted in heptol

(80:20). This observation further acknowledges the absence of asphaltenes aggregation/precipitation in the case of 40 wt.% bitumen diluted in heptol (80:20).

By measuring bulk contact angle of bitumen solutions on the etched surface of glass as described in the section 3.2.5, we noticed that as bitumen concentration goes up the contact angle also increases. This observation suggests that solution hydrophobicity will be affected by the bitumen content in the studied solvent. The degree of hydrophobicity increases with increase in the bitumen concentration. The measured contact angle for 5 and 40 wt.% bitumen diluted in heptol (80:20) is shown in Figure 3.17 and Figure 3.18. The results for measured physical properties of different liquids and the theoretical values are summarized in Table 3.1.

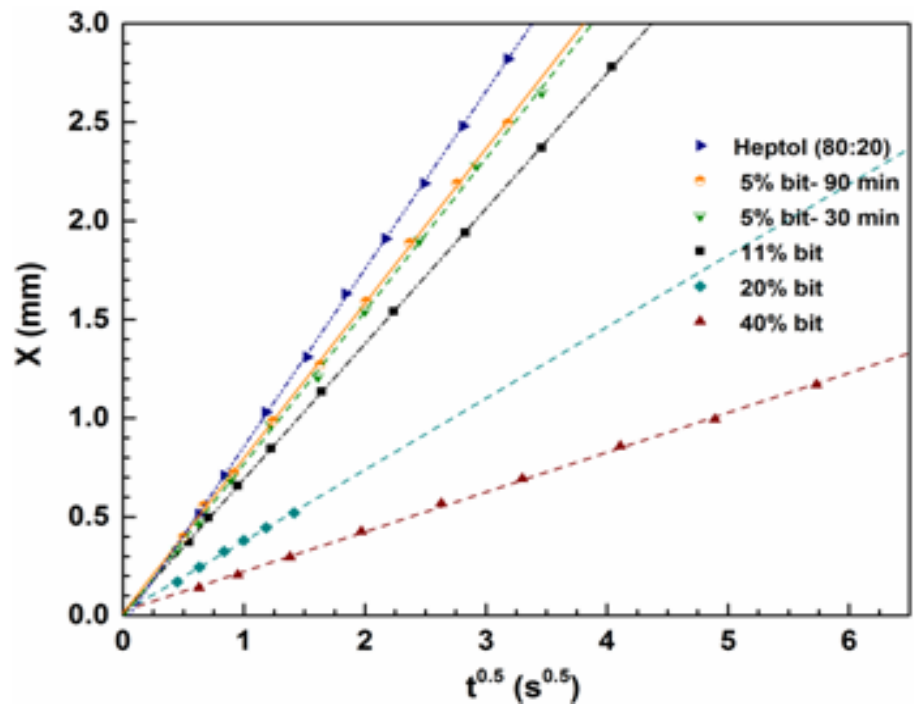


Figure 3.9. The Penetration of bitumen solutions diluted in heptol (80:20) as a function of $t^{0.5}$ in nanochannel with the depth and width of 47 nm and 15 μm , respectively.

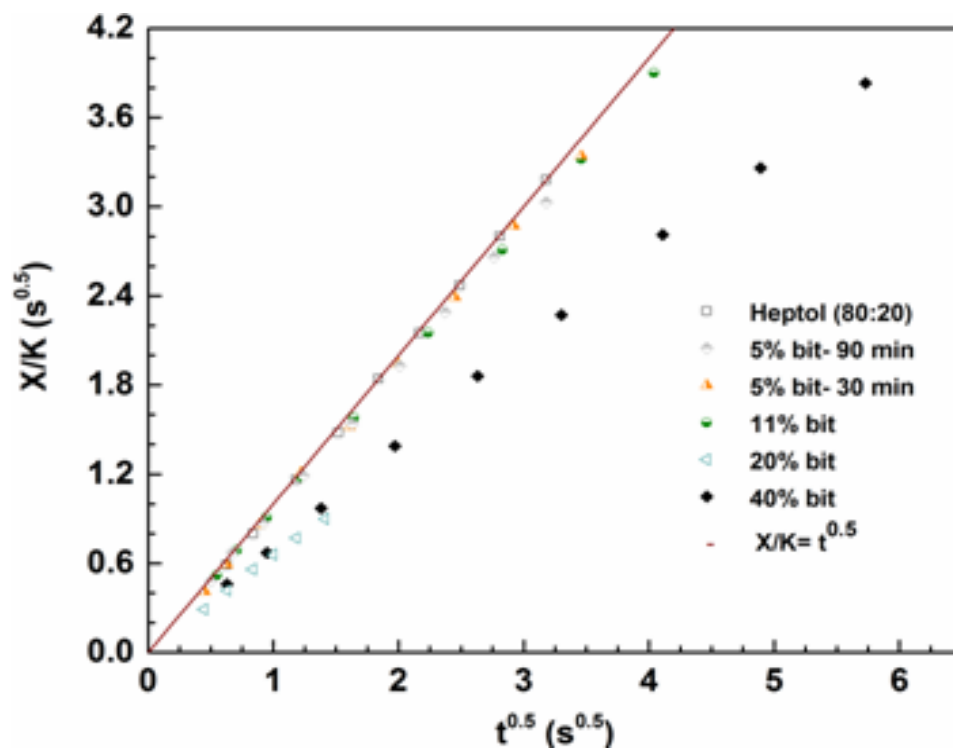


Figure 3.10. The variation of x/k as a function of $t^{0.5}$ for capillary flow of bitumen solutions diluted in heptol (80:20) in nanochannel with the depth and width of 47 nm and 15 μ m, respectively.

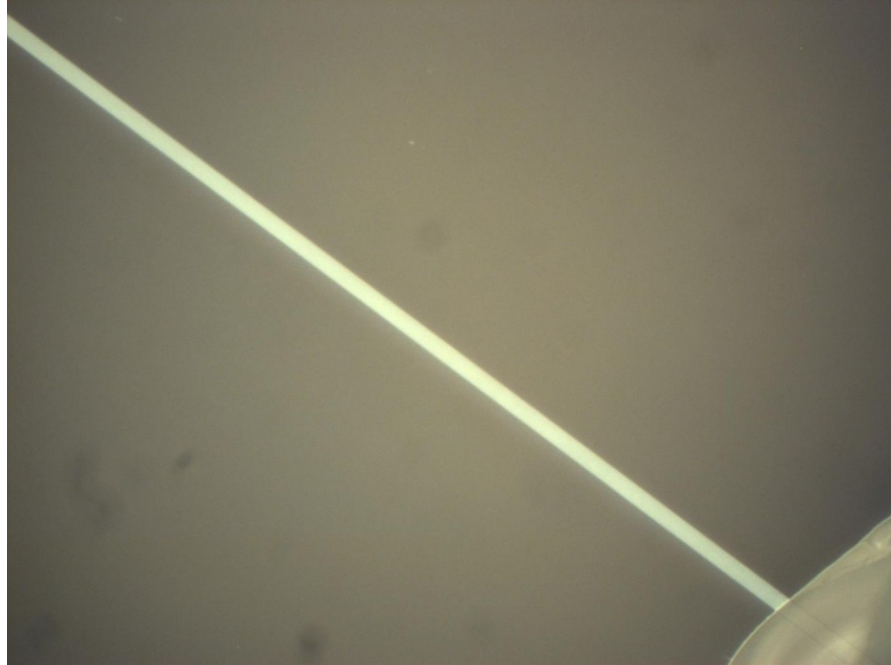


Figure 3.11. Empty Reservoir before filling with 40% bitumen.

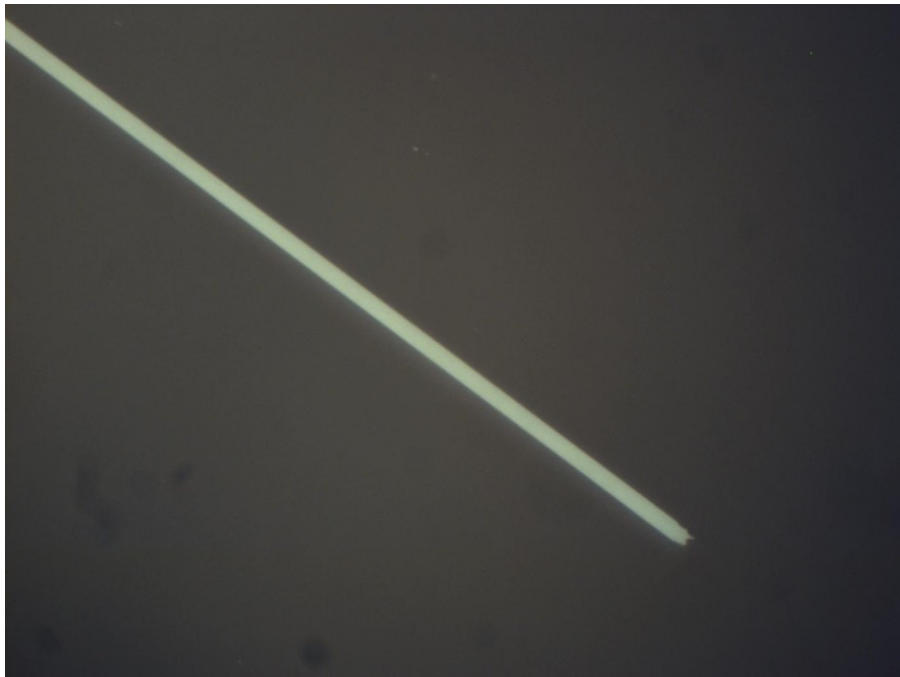


Figure 3.12. Capillary filling of 40 wt.% bitumen diluted in heptol (80:20) at $t= 0.3$ s.



Figure 3.13. Capillary filling of 40 wt.% bitumen diluted in heptol (80:20) at $t= 1.4$ s.

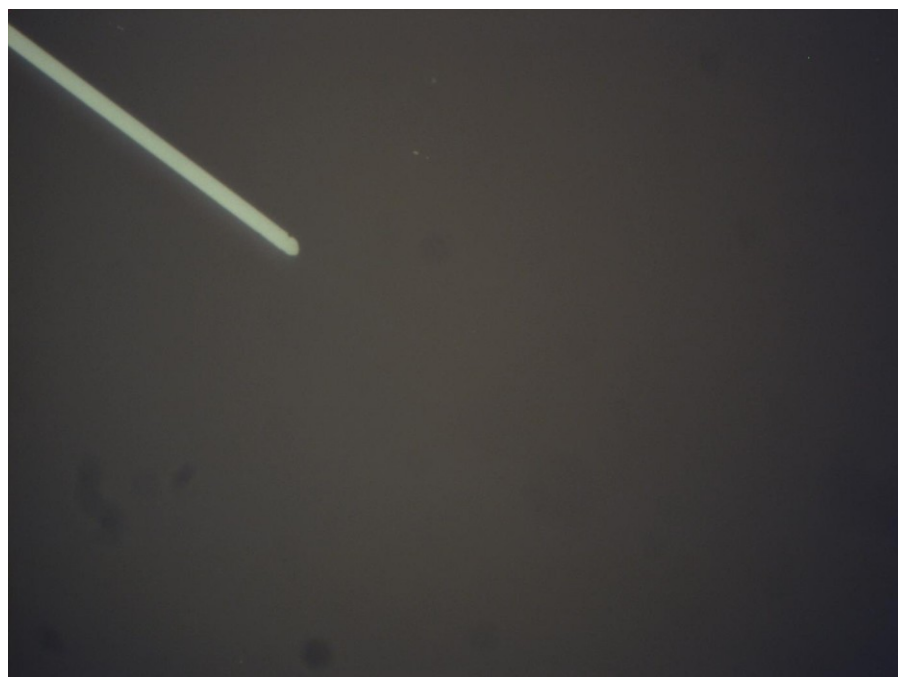


Figure 3.14. Capillary filling of 40 wt.% bitumen diluted in heptol (80:20) at $t= 6.7$ s.

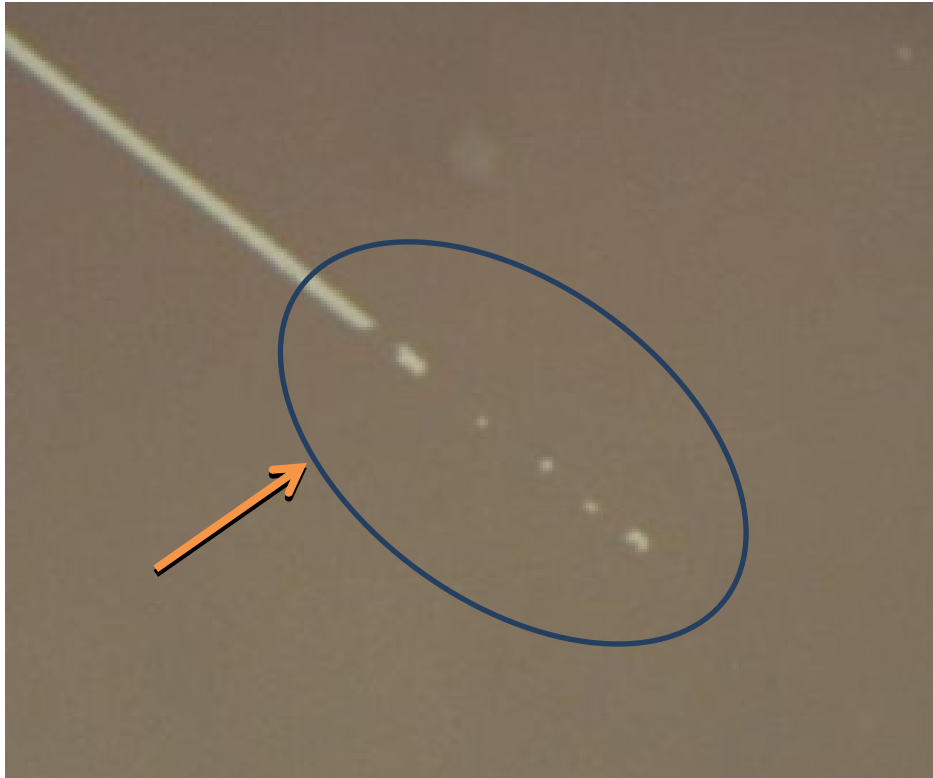


Figure 3.15. Formation of air bubbles during capillary filling of 20 wt.% bitumen diluted in heptol (80:20).

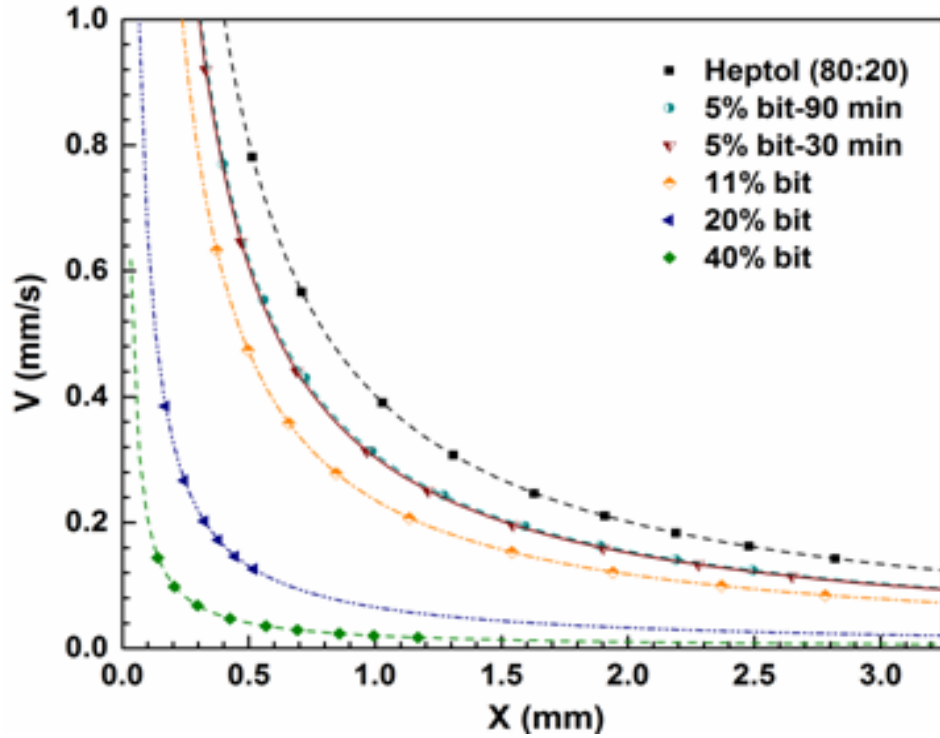


Figure 3.16. The velocity of advancing bitumen solutions diluted in heptol (80:20) as a function of penetration distance in nanochannel with the depth and width of 47 nm and 15 μm , respectively.



Figure 3.17. The measured bulk contact angle of 40 wt.% bitumen in heptol (80:20) on borofloat glass 0.3 s after the contact. The mean contact angle was about 26 degree.

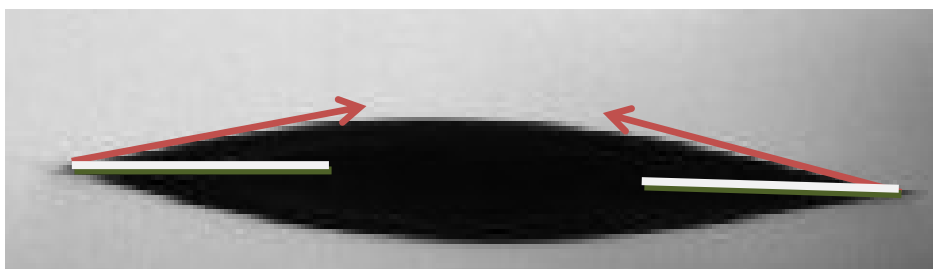


Figure 3.18. The measured bulk contact angle of 5 wt.% bitumen in heptol (80:20) on borofloat glass 0.3 s after the contact. The mean contact angle was about 12 degree.

Liquid	Surface tension (mN/m)	Bulk contact angle (θ_b)	Depth (nm)	Theoretical viscosity (mPa·s)	Measured bulk viscosity (mPa·s)
Water	72.2	15	47	1.52	0.96
Methanol	22.8	7	47	0.59	0.58
Ethanol	22.2	9	47	1.46	1.40
Heptol (80:20)	22.5	11	47	0.43	0.44
5% bitumen-90 min	21.8	12	47	0.54	0.50
5% bitumen-30 min	21.8	12	47	0.55	0.51
11% bitumen	21.7	14	47	0.70	0.64
20% bitumen	21.1	18	47	2.40	0.90
40% bitumen	19	26	47	6.6	2.8

Table 3.1. The values of different liquids physical properties.

3.4.3. Capillary-Driven Flow of Bingham Plastic Fluid

As already mentioned in the Introduction part, above the critical solvent to bitumen ratio (S/B), asphaltenes form aggregates. In the recent studies, it was proposed that formation of asphaltenes aggregates at the W/O interface prevents

the thin oil film breakage when two water droplets approaching each other.¹¹ The oil film drainage stops at the thickness less than 100 nm. The reason behind this observation was attributed to the change in the rheology of thin oil film from Newtonian to non-Newtonian Bingham Plastic as a result of asphaltene aggregation. The schematic of oil film drainage from the study of W/O emulsion is illustrated in Figure 3.19.¹¹ In this section, our objective was to examine a possible Bingham Plastic behavior of oil film in the presence of asphaltene aggregation in the same scale (less than 100 nm) as oil film drainage stops.

The experiments were conducted with the similar conditions (i.e. same bitumen concentration and temperature) as the non-Newtonian Bingham Plastic behavior of thin oil film was reported. We also chose glass chip as the glass surface has the hydrophilic nature similar to the water droplets. Furthermore, as already mentioned in Section 3.3.2, the related equations for capillary filling of Bingham Plastic flow were developed to help us analyze the experimental results. Figure 3.20 shows the theoretical predictions for Bingham Plastic fluid with different values of yield stress (τ_0). It is clear that as the value of τ_0 increase the non-linear relationship between penetration distance and square root of time becomes more distinctive. The reported value of yield stress in the drainage study of thin oil film was less than about 0.1 Pa. By comparing the experimental data in the case of 5 wt.% bitumen diluted in heptol (80:20) with the theoretical predictions of Newtonian and non-Newtonian Bingham Plastic fluid (when τ_0 is equal to 0.1 Pa), it is difficult to acknowledge that 5 wt.% bitumen diluted in heptol (80:20) demonstrates a Bingham Plastic behavior in the nano-confinement

geometry. If the bitumen sample could penetrate for a longer time, we might be able to determine whether the bitumen sample is non-Newtonian or not. However, due to the technical problems such as nanochannel blockage and some defects in the fabricated nanochannels during the capillary filling process, we could not conduct the experiments for a longer time.

The meniscus velocity of a Bingham Plastic fluid as a function of penetration distance is plotted in Figure 3.21. The graph shows that the velocity decreases faster for the larger values of τ_0 . It can be noted that the difference between Bingham Plastic fluids with different values of τ_0 is more noticeable in Figure 3.20, where penetration distance is plotted versus square root of time in comparison with Figure 3.21.

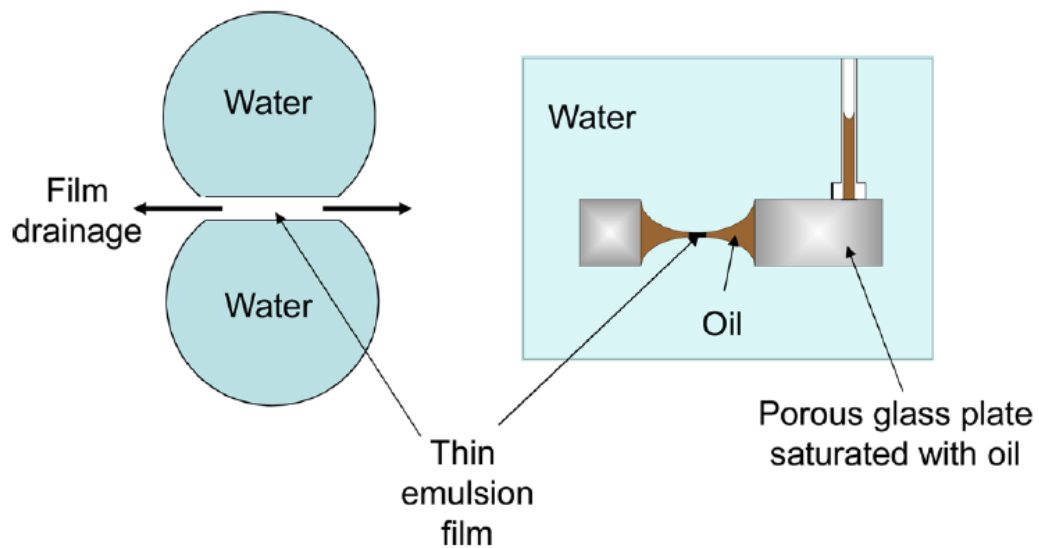


Figure 3.19. Schematic of thin oil film drainage from W/O emulsion study.¹¹

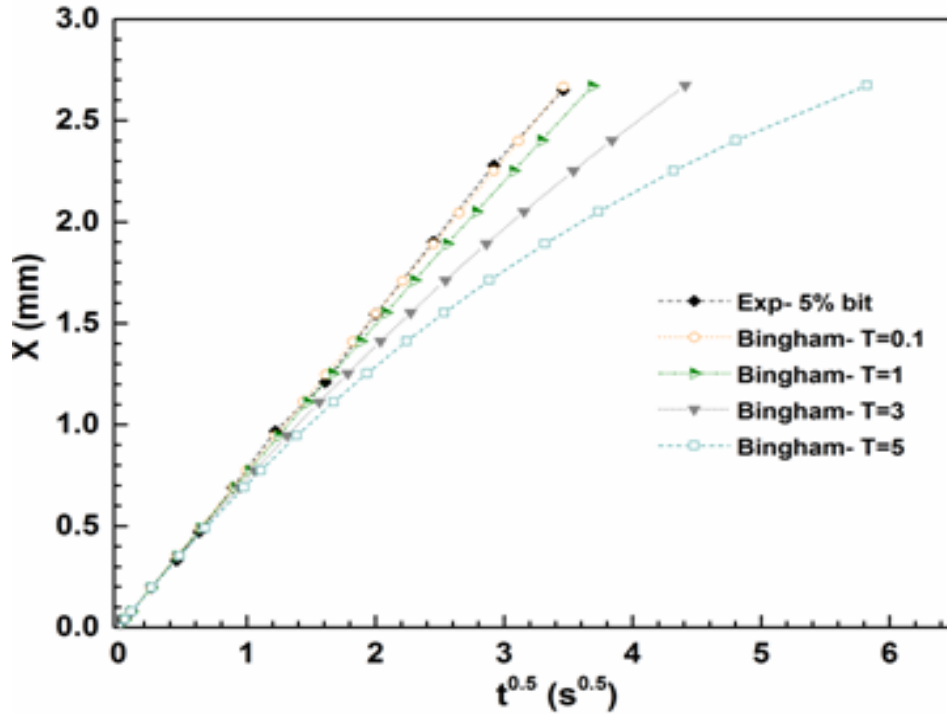


Figure 3.20. The theoretical prediction of Bingham Plastic flow penetration as a function of $t^{0.5}$ distance in nanochannel with the depth and width of 47 nm and 15 μm , respectively.

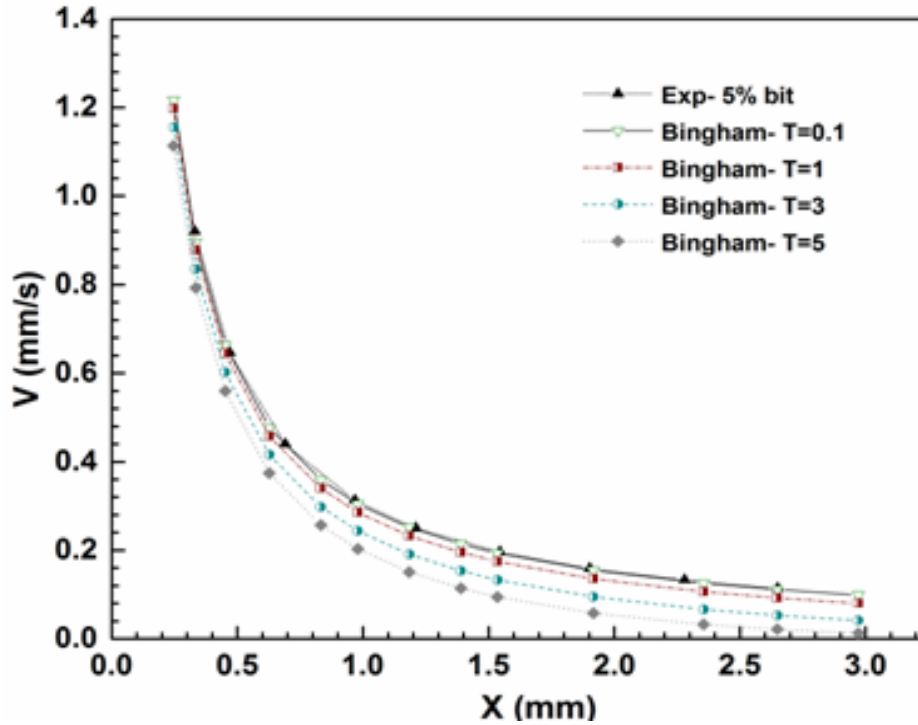


Figure 3.21. The theoretical prediction of Bingham Plastic velocity as a function of penetration distance in nanochannel with the depth and width of 47 nm and 15 μm , respectively.

3.5. CONCLUSION

Capillary filling process of different liquids was performed in the 47 nm deep and 15 μm wide nanochannels. In the case of pure liquids (water, ethanol, and methanol), the position of advancing meniscus changed linearly with the square root of time which is the character of Newtonian fluid. Filling kinetics of ethanol and methanol agreed well with the theoretical models. However, water demonstrated lower filling rates in comparison with the theoretical values. For 20 and 40 wt.% bitumen diluted in heptol (80:20), the large variation in dynamic contact angle was observed that is the reason for substantial deviation from the

theoretical predictions. In the case of 20 wt.% diluted bitumen, the presence of asphaltene aggregates often led to fast blockage of nanochannel. Asphaltene aggregates may also limit the liquid flow and cause air bubbles formation. For 40 wt.% diluted bitumen, much longer penetration time was noticed compared to 20 wt.% diluted bitumen. This observation further proves the absence of asphaltene aggregates in the 40 wt.% bitumen sample. Theoretical models were developed to predict the capillary filling kinetics of Bingham Plastic fluid in the nanochannels. It was noticed as the value of yield stress increases, the non-linear relationship between position of advancing meniscus and square root of time becomes more pronounced. Furthermore, when the value of yield stress was less than about 0.1 Pa, it became hard to differentiate between Newtonian and Bingham Plastic fluid behavior. Nanochannels can be a suitable model to analyze the flow of heavy oil in the nano-porous media like rocks.

Chapter 4. Conclusions and Future Work

4.1 Concluding Remarks

The work presented in this thesis is mainly focused on the rheology study of diluted Athabasca bitumen above and below the critical S/B ratio in macro- and nano-confinement scale. Conventional rheometer is used to study the bulk rheology of bitumen solutions in different type of solvents. Finally, nanofluidic devices are fabricated based on well-defined nanofabrication techniques which enable us to perform rheological analysis of desired fluid in the nanoscale not possible using conventional rheometer. The main conclusions of the conducted research in this thesis are listed below.

- Above the critical S/B ratio, asphaltenes initially form nano-aggregates. These nano-aggregates form larger structures called clusters which grow to the large asphaltene particles and eventually precipitate out of the bitumen solutions.
- Viscosity of bitumen solutions diluted in heptane and heptol (80:20) above the critical S/B ratio decreased with aging time up to several days. The reduction in the viscosity was attributed to the formation of asphaltene aggregates, which ultimately precipitated out and consequently decreased the bitumen volume fraction in the solutions.

- Time dependency of the viscosity reduction further indicates that the formation of asphaltene aggregates/precipitates is a continuous process which has a time scale of about weeks.⁹⁸
- Viscosity of bitumen solutions diluted in heptane and heptol (80:20) below the critical S/B ratio and also in toluene did not change with aging time. This observation suggests that the formation of large asphaltene aggregates/precipitates did not occur in these solutions.
- Rate of asphaltenes aggregation/precipitation depends on the solvent composition (degree of aromaticity). Based on viscosity modeling and experimental observation, the higher precipitation rate was observed in the case of heptane compared to heptol (80:20).
- All bitumen solutions diluted in different solvents at the room temperature demonstrated a Newtonian fluid behavior regardless of the critical S/B ratio.
- Ultra-low aspect ratio nanochannels made out of glass enabled us to easily monitor the capillary filling process of pure liquids and bitumen solutions in the nano-confinement geometry. Furthermore, the theoretical analysis was eased as ultra-low aspect ratio nanochannels could be modeled as 1-D systems.
- To analyze the flow in our nanofluidic system, capillary-driven flow was selected since it did not require pump for fluid transport and could be applied to any type of solvents.

- Filling kinetics of bitumen solutions diluted in heptol (80:20) with low bitumen concentration (less than about 11 wt.%) is in good agreement with the theoretical predictions. Nevertheless, for 20 and 40 wt.% bitumen diluted in heptol (80:20), considerable deviation from the theory was observed. For all bitumen solutions during capillary filling process, the position of advancing meniscus linearly changed with the square root of time that implied the bitumen solutions behave similar to the Newtonian fluid.
- The filling speed of 20 and 40 wt.% bitumen diluted in heptol (80:20) was found to be much lower than the theoretical values. This deviation was attributed to the large variation in the dynamic contact angle of advancing meniscus. Therefore, the assumption of constant contact angle during capillary filling phenomena was incorrect.
- Formation of asphaltene aggregates in the case of 20 wt.% bitumen diluted in heptol (80:20) often blocked the nanochannels path and led to short penetration distance. Moreover, the air bubbles were formed in the nanochannels. This might occur due to the presence of aggregates which limit the fluid flow. However, these phenomena were not observed for 40 wt.% bitumen diluted in heptol (80:20) which confirms the absence of asphaltene aggregates in the bitumen solutions below the critical S/B ratio.
- The theoretical predictions for capillary filling kinetics of Bingham Plastic fluid in the nanochannel were developed to examine a possible

non-Newtonian Bingham Plastic rheology in the bitumen solutions above the critical S/B ratio.

- In the case of Bingham Plastic fluid, we noticed as the value of yield stress increased the non-linear relationship between penetration distance of advancing liquid and square root of time became more distinguishable.
- Since in the case of bitumen solutions above the critical S/B ratio, the reported values of Bingham yield stress was less than about 0.1 Pa, it was difficult to distinguish between Newtonian and Bingham Plastic rheology. Therefore, we could not determine if 5 wt.% bitumen diluted in heptol (80:20) is Bingham Plastic fluid in the nano-confinement geometry or not.
- We had a hypothesis that asphaltene aggregation might change the rheology of bitumen. We took a macroscopic approach as well as a nanoscopic approach. Both techniques have a detection limit for yield stress, and so far considering their detection limit, we have not measured any yield stress. This implies that aggregation does not seem to change the rheology of bitumen, or even if it does, the effect is too small to detect.

4.2 Future Work

For the future investigations in the field, the following recommendations and suggestions are presented that might help to answer some of the unresolved problems.

- In fact, the bulk rheology of bitumen solutions above and below the critical S/B ratio was performed under ambient conditions. The effect of different temperatures and pressures on bitumen rheology can be studied. It also reveals how the aggregation mechanism of asphaltenes might be affected under different conditions.
- We estimated the small volume fraction of dispersed asphaltenes in the bitumen solutions based on simple and well-known viscosity models available in the literature. However, there are experimental methods that can be used for determination of asphaltenes content in the bitumen solutions and might provide more accurate data.
- In the study of capillary filling kinetics in the nanofluidic system, the width and depth size of fabricated nanochannels were fixed. However, nanochannels with different size of depth and width can be fabricated to examine the effect of channel size on the capillary filling kinetics of various solutions.
- Nanofluidic chips were made out of the glass substrates. The glass acquires a hydrophilic surface. It would be interesting to alter the glass surface properties through the surface treatment and make the surface hydrophobic. Afterwards, the change in the dynamic contact angle of advancing meniscus and subsequently in the meniscus filling speed can be studied.
- In our study, the capillary-driven flow was used to transport the fluid in the nanochannels. As it was mentioned in the Chapter 3, the contact

angle variation during capillary filling is problematic since in the theoretical predictions, the dynamic contact angle is assumed to be constant which in reality it is not. Pressure-driven flow can be used to study the fluid rheology. The advantage of this method is that it is independent of contact angle. However, it is worth to mention that in the case of bitumen solutions nanochannels with larger cross-sectional area are needed to reduce the high pressure drop and prevent channel blockage.

References

1. Kilpatrick, P. K. and Spiecker, P. M., *Asphaltene emulsions*. **In Encyclopedic Handbook of Emulsion Technology**, Sjoblom, J., Ed. Marcel Dekker: New York, 2001, Vol. 3, pp 707-730.
2. Kilpatrick, P. K., *Water-in-Crude Oil Emulsion Stabilization: Review and Unanswered Questions*. **Energy & Fuels**, 2012, 26, (7), 4017-4026.
3. Brennan, J. G. and Grandison, A. S., *Food Processing Handbook*. **Wiley**: 2012.
4. Czarnecki, J., *Water-in-oil emulsions in recovery of hydrocarbons from oil sands*. **In Encyclopedic Handbook of Emulsion Technology**, Sjoblom, J., Ed. Marcel Dekker: New York, Basel, 2001, pp 497-514.
5. Masliyah, J., Czarnecki, J. and Xu, Z., *Handbook on Theory and Practice of Bitumen Recovery from Athabasca Oil Sands*. **Kingsley Knowledge Publishing**: Cochrane, Canada, 2011.
6. Hemmingsen, P. V., Silset, A., Hannisdal, A. and Sjöblom, J., *Emulsions of Heavy Crude Oils. I: Influence of Viscosity, Temperature, and Dilution*. **Journal of Dispersion Science and Technology**, 2005, 26, (5), 615-627.
7. Yan, Z., Elliott, J. A. and Masliyah, J. H., *Roles of Various Bitumen Components in the Stability of Water-in-Diluted-Bitumen Emulsions*. **J Colloid Interface Sci**, 1999, 220, (2), 329-337.
8. Poteau, S., Argillier, J. F., Langevin, D., Pincet, F., Perez, E., *Influence of pH on Stability and Dynamic Properties of Asphaltenes and Other*

- Amphiphilic Molecules at the Oil–Water Interface*, **Energy & Fuels**, 2005, 19, (4), 1337-1341.
9. Horváth-Szabó, G., Masliyah, J. H., Czarnecki, J., *Phase Behavior of Sodium Naphthenates, Toluene, and Water*. **Journal of Colloid and Interface Science**, 2001, 242, (1), 247-254.
10. Gafonova, O. V. and Yarranton, H. W., *The Stabilization of Water-in-Hydrocarbon Emulsions by Asphaltenes and Resins*. **Journal of Colloid and Interface Science**, 2001, 241, (2), 469-478.
11. Czarnecki, J., Tchoukov, P. and Dabros, T., *Possible Role of Asphaltenes in the Stabilization of Water-in-Crude Oil Emulsions*. **Energy & Fuels**, 2012, 26, (9), 5782-5786.
12. Tchoukov, P., Yang, F., Xu, Z., Dabros, T., Czarnecki, J. and Sjoblom, J., *Role of asphaltenes in stabilizing thin liquid emulsion films*. **Langmuir**, 2014, 30, (11), 3024-33.
13. Andreatta, G., Bostrom, N. and Mullins, O. C., *High-Q ultrasonic determination of the critical nanoaggregate concentration of asphaltenes and the critical micelle concentration of standard surfactants*. **Langmuir**, 2005, 21, (7), 2728-36.
14. Mullins, O. C., *The Asphaltenes*. **Annual Review of Analytical Chemistry**, 2011, 4, (1), 393-418.
15. Sheu, E. Y., *Petroleum asphaltene-properties, characterization, and issues*. **Energy & Fuels**, 2002, 16, (1), 74-82.

16. Angle, C. W., Lue, L., Dabros, T. and Hamza, H. A., *Viscosities of Heavy Oils in Toluene and Partially Deasphalted Heavy Oils in Heptol in a Study of Asphaltenes Self-Interactions*. **Energy & Fuels**, 2005, 19, (5), 2014-2020.
17. Hasan, M. D. A., Fulem, M., Bazyleva, A. and Shaw, J. M., *Rheological Properties of Nanofiltered Athabasca Bitumen and Maya Crude Oil*. **Energy & Fuels**, 2009, 23, 5012-5021.
18. Alomair, O. A. and Almusallam, A. S., *Heavy Crude Oil Viscosity Reduction and the Impact of Asphaltene Precipitation*. **Energy & Fuels**, 2013, 27, (12), 7267-7276.
19. Carlomagno, G. M., *Computational Methods and Experimental Measurements XV*. **WIT Press**: 2011, Southampton, UK.
20. Tchoukov, P., Czarnecki, J. and Dabros, T., *Study of water-in-oil thin liquid films: Implications for the stability of petroleum emulsions*. **Colloids and Surfaces A: Physicochemical and Engineering Aspects**, 2010, 372, (1–3), 15-21.
21. Yeung, A., Dabros, T., Czarnecki, J. and Masliyah, J., *On the interfacial properties of micrometre-sized water droplets in crude oil*. **Proceedings of the Royal Society of London. Series A: Mathematical, Physical and Engineering Sciences**, 1999, 455, (1990), 3709-3723.
22. Czarnecki, J. and Moran, K., *On the stabilization mechanism of water-in-oil emulsions in petroleum systems*. **Energy & Fuels**, 2005, 19, (5), 2074-2079.

23. Dabros, T., Yeung, A., Masliyah, J. and Czarnecki, J., *Emulsification through area contraction*. **Journal of Colloid and Interface Science**, 1999, 210, (1), 222-224.
24. Spiecker, P. M., and Kilpatrick, P. K., *Interfacial rheology of petroleum asphaltenes at the oil-water interface*. **Langmuir**, 2004, 20, (10), 4022-4032.
25. Abdul-Raouf, M. E. S., *Factors Affecting the Stability of Crude Oil Emulsions. Crude Oil Emulsions- Composition Stability and Characterization*, **InTech**, 2012, DOI: 10.5772/35018
26. Mohammed, R. A., Bailey, A. I., Luckham, P. F., Taylor, S. E., *Dewatering of crude oil emulsions 1. Rheological behaviour of the crude oil—water interface*. **Colloids and Surfaces A: Physicochemical and Engineering Aspects**, 1993, 80, (2–3), 223-235.
27. Sun, T., Zhang, L., Wang, Y., Zhao, S., Peng, B., Li, M., Yu, J., *Influence of demulsifiers of different structures on interfacial dilational properties of an oil-water interface containing surface-active fractions from crude oil*. **J Colloid Interface Sci**, 2002, 255, (2), 241-7.
28. Mozaffari, S., Czarnecki, J. and Nazemifard, N. *Nanofluidic platform for water-in-oil emulsion stability analysis*. **Proceeding of the 64th Canadian Chemical Engineering Conference**, 2014, Niagara Falls, Canada.
29. Sparreboom, W., Berg, A. v. d., and Eijkel, J. C. T., *Transport in nanofluidic systems: a review of theory and applications*. **New Journal of Physics**, 2010, 12, (1), 015004.

30. Eijkel, J. T. and Berg, A., *Nanofluidics: what is it and what can we expect from it?* **Microfluidics and Nanofluidics**, 2005, 1, (3), 249-267.
31. Duan, C., Wang, W., and Xie, Q., *Review article: Fabrication of nanofluidic devices.* **Biomicrofluidics**, 2013, 7, (2), 26501.
32. Andersson, H., and van den Berg, A., *Microtechnologies and nanotechnologies for single-cell analysis.* **Current Opinion in Biotechnology**, 2004, 15, (1), 44-49.
33. Kim, S. J., Ko, S. H., Kang, K. H. and Han, J., *Direct seawater desalination by ion concentration polarization.* **Nat Nano**, 2010, 5, (4), 297-301.
34. Saleh, O. A., and Sohn, L. L., *An artificial nanopore for molecular sensing.* **Nano Letters**, 2003, 3, (1), 37-38.
35. Daiguji, H., Yang, P., Szeri, A. J., and Majumdar, A., *Electrochemomechanical Energy Conversion in Nanofluidic Channels.* **Nano Letters**, 2004, 4, (12), 2315-2321.
36. Gates, B. D., Xu, Q. B., Stewart, M., Ryan, D., Willson, C. G., and Whitesides, G. M., *New approaches to nanofabrication: Molding, printing, and other techniques.* **Chemical Reviews**, 2005, 105, (4), 1171-1196.
37. Seeman, N. C., *At the Crossroads of Chemistry, Biology, and Materials: Structural DNA Nanotechnology.* **Chemistry & Biology**, 2003, 10, (12), 1151-1159.
38. Abgrall, P., and Nguyen, N. T., *Nanofluidic devices and their applications.* **Analytical Chemistry**, 2008, 80, (7), 2326-2341.

39. Pinti, M., Kambham, T., Wang, B. and Prakash, S., *Fabrication of Centimeter Long, Ultra-Low Aspect Ratio Nanochannel Networks in Borosilicate Glass Substrates*. **Journal of Nanotechnology in Engineering and Medicine**, 2013, 4, (2), 020905-020905.
40. Pinti, M., and Prakash, S.; *A Two-Step Wet Etch Process for the Facile Fabrication of Hybrid Micro-Nanofluidic Devices*. **American Society of Mechanical Engineers**, 2012; p 647-651.
41. Bayraktar, T., and Pidugu, S. B., *Characterization of liquid flows in microfluidic systems*. **International Journal of Heat and Mass Transfer**, 2006, 49, (5–6), 815-824.
42. Tamaki, E., Hibara, A., Kim, H. B., Tokeshi, M., and Kitamori, T., *Pressure-driven flow control system for nanofluidic chemical process*. **Journal of Chromatography A**, 2006, 1137, (2), 256-262.
43. Kim, P., Kim, H. Y., Kim, J. K., Reiter, G., and Suh, K. Y., *Multi-curvature liquid meniscus in a nanochannel: Evidence of interplay between intermolecular and surface forces*. **Lab on a Chip**, 2009, 9, (22), 3255-3260.
44. Tas, N. R., Haneveld, J., Jansen, H. V., Elwenspoek, M., and van den Berg, A., *Capillary filling speed of water in nanochannels*. **Applied Physics Letters**, 2004, 85, (15), 3274-3276.
45. Kuo, J. N., and Lin, Y. K., *Capillary-Driven Dynamics of Water in Hydrophilic Microscope Coverslip Nanochannels*. **Japanese Journal of Applied Physics**, 2012, 51, (10).

46. Washburn, E. W., *The Dynamics of Capillary Flow*. **Physical Review** 1921, 17, (3), 273-283.
47. Han, A., Mondin, G., Hegelbach, N. G., de Rooij, N. F., and Staufer, U., *Filling kinetics of liquids in nanochannels as narrow as 27 nm by capillary force*. **Journal of Colloid and Interface Science**, 2006, 293, (1), 151-157.
48. Zhu, Y., and Petkovic-Duran, K., *Capillary flow in microchannels*. **Microfluidics and Nanofluidics**, 2010, 8, (2), 275-282.
49. Mouazen, M., Poulesquen, A., Bart, F., Masson, J., Charlot, M., and Vergnes, B., *Rheological, structural and chemical evolution of bitumen under gamma irradiation*. **Fuel Processing Technology**, 2013, 114, 144-153.
50. Lemarchand, C. A., Schroder, T. B., Dyre, J. C., and Hansen, J. S., *Cooee bitumen: chemical aging*. **J Chem Phys**, 2013, 139, (12), 124506.
51. Yen, T. F., and Chilingarian, G. V., *Asphaltenes and Asphalts, 2*. **Elsevier Science**, 2000.
52. Sheu, E., and Mullins, O., *Asphaltenes : fundamentals and applications*. **Plenum Press**, 1995; p 245.
53. Xu, Y., Dabros, T., Hamza, H., and Shefantook, W., *Destabilization of water in bitumen emulsion by washing with water*. **Petroleum Science and Technology**, 1999, 17, (9-10), 1051-1070.
54. Branco, V. A. M, Mansoori, G. A., De Almeida Xavier, L. C., Park, S. J., and Manafi, H., *Asphaltene flocculation and collapse from petroleum fluids*. **Journal of Petroleum Science and Engineering**, 2001, 32, (2-4), 217-230.

55. Pal, R., *A new model for the viscosity of asphaltene solutions*. **The Canadian Journal of Chemical Engineering**, 2015, 93, (4), 747-755.
56. Mitchell, D. L., and Speight, J. G., *The solubility of asphaltenes in hydrocarbon solvents*. **Fuel**, 1973, 52, (2), 149-152.
57. Sirota, E. B., and Lin, M. Y., *Physical behavior of asphaltenes*. **Energy & Fuels**, 2007, 21, (5), 2809-2815.
58. Hasan, M. D. A., and Shaw, J. M., *Rheology of Reconstituted Crude Oils: Artifacts and Asphaltenes*. **Energy & Fuels**, 2010, 24, (12), 6417-6427.
59. Edwards, Y., and Redelius, P., *Rheological Effects of Waxes in Bitumen*. **Energy & Fuels**, 2003, 17, (3), 511-520.
60. Spiecker, P. M., Gawrys, K. L., and Kilpatrick, P. K., *Aggregation and solubility behavior of asphaltenes and their subfractions*. **J Colloid Interface Sci**, 2003, 267, (1), 178-93.
61. Murgich, J., and Strausz, O. P., *Molecular Mechanics of Aggregates of Asphaltenes and Resins of the Athabasca Oil*. **Petroleum Science and Technology**, 2001, 19, (1-2), 231-243.
62. Eyssautier, J., Levitz, P., Espinat, D., Jestin, J., Gummel, J., Grillo, I., and Barre, L., *Insight into Asphaltene Nanoaggregate Structure Inferred by Small Angle Neutron and X-ray Scattering*. **Journal of Physical Chemistry B**, 2011, 115, (21), 6827-6837.
63. Bouhadda, Y., Bendedouch, D., Sheu, E., and Krallafa, A., *Some Preliminary Results on a Physico-Chemical Characterization of a Hassi Messaoud Petroleum Asphaltene*. **Energy & Fuels**, 2000, 14, (4), 845-853.

64. Eyssautier, J., Hénaut, I., Levitz, P., Espinat, D., and Barré, L., *Organization of Asphaltenes in a Vacuum Residue: A Small-Angle X-ray Scattering (SAXS)–Viscosity Approach at High Temperatures*. **Energy & Fuels**, 2012, 26, (5), 2696-2704.
65. McLean, J. D., and Kilpatrick, P. K., *Effects of Asphaltene Solvency on Stability of Water-in-Crude-Oil Emulsions*. **Journal of Colloid and Interface Science**, 1997, 189, (2), 242-253.
66. McLean, J. D., and Kilpatrick, P. K., *Effects of asphaltene aggregation in model heptane–toluene mixtures on stability of water-in-oil emulsions*. **Journal of Colloid and Interface Science**, 1997, 196, (1), 23-34.
67. Czarnecki, J., Tchoukov, P., Dabros, T., and Xu, Z. H., *Role of asphaltenes in stabilisation of water in crude oil emulsions*. **Canadian Journal of Chemical Engineering**, 2013, 91, (8), 1365-1371.
68. Long, Y., Dabros, T., Hamza, H., and Power, W. J. *Reversibility of asphaltene precipitation from paraffinic solvent-diluted bitumen*, **Proceeding of the 50th Canadian Chemical Engineering Conference**, 2000, Montreal, Canada.
69. Yen, T. F., Erdman, J. G., and Pollack, S. S., *Investigation of the Structure of Petroleum Asphaltenes by X-Ray Diffraction*. **Analytical Chemistry**, 1961, 33, (11), 1587-1594.
70. Pal, R., *A new model for the viscosity of asphaltene solutions*. **The Canadian Journal of Chemical Engineering**, 2015, 93, (4), 747-755.

71. Woutersen, A. T. J. M., and de Kruif, C. G., *The viscosity of semidilute, bidisperse suspensions of hard spheres*. **Journal of Rheology (1978-present)**, 1993, 37, (4), 681-693.
72. Liu, S., and Masliyah Jacob, H., *Rheology of Suspensions*. In *Suspensions: Fundamentals and Applications in the Petroleum Industry*, **American Chemical Society**, 1996; Vol. 251, pp 107-176.
73. Selim, M. S., Al-Naafa, M. A., and Jones, M. C., *Brownian diffusion of hard spheres at finite concentrations*. **AIChE Journal**, 1993, 39, (1), 3-16.
74. Roscoe, R., *The viscosity of suspensions of rigid spheres*. **British Journal of Applied Physics**, 1952, 3, (8), 267.
75. Pal, R., and Rhodes, E., *Viscosity/Concentration Relationships for Emulsions*. **Journal of Rheology**, 1989, 33, (7), 1021-1045.
76. Krieger, I. M., *Rheology of monodisperse latices*. **Advances in Colloid and Interface Science**, 1972, 3, (2), 111-136.
77. Zeng, H., and Zhao, Y., *Rheological analysis of non-Newtonian blood flow using a microfluidic device*. **Sensors and Actuators A: Physical**, 2011, 166, (2), 207-213.
78. Han, J., and Craighead, H. G., *Separation of Long DNA Molecules in a Microfabricated Entropic Trap Array*. **Science**, 2000, 288, (5468), 1026-1029.
79. Sinha, P. M., Valco, G., Sharma, S., Liu, X., and Ferrari, M., *Nanoengineered device for drug delivery application*. **Nanotechnology**, 2004, 15, (10), S585.

80. Prakash, S., Karacor, M. B., and Banerjee, S., *Surface modification in microsystems and nanosystems*. **Surface Science Reports**, 2009, 64, (7), 233-254.
81. Mao, P., and Han, J., *Fabrication and characterization of 20 nm planar nanofluidic channels by glass-glass and glass-silicon bonding*. **Lab Chip**, 2005, 5, (8), 837-44.
82. Lin, C.H., Lee, G.B., Lin, Y.H., and Chang, G.L., *A fast prototyping process for fabrication of microfluidic systems on soda-lime glass*. **Journal of Micromechanics and Microengineering**, 2001, 11, (6), 726.
83. Kuo, J.N., Lin, and Y.K., *Fabrication of 20 nm Shallow Nanofluidic Channels Using Coverslip Thin Glass–Glass Fusion Bonding Method*. **Japanese Journal of Applied Physics**, 2012, 51, (9R), 095202.
84. Pinti, M., and Prakash, S. *Fabrication of Hybrid Micro-Nanofluidic Devices With Centimeter Long Ultra-Low Aspect Ratio Nanochannels*, **American Society of Mechanical Engineers**, 2014, pp. V010T11A045.
85. Hibara, A., Saito, T., Kim, H. B., Tokeshi, M., Ooi, T., Nakao, M., and Kitamori, T., *Nanochannels on a fused-silica microchip and liquid properties investigation by time-resolved fluorescence measurements*. **Analytical Chemistry**, 2002, 74, (24), 6170-6176.
86. Rossi, M. P., Ye, H. H., Gogotsi, Y., Babu, S., Ndungu, P., and Bradley, J. C., *Environmental scanning electron microscopy study of water in carbon nanopipes*. **Nano Letters**, 2004, 4, (5), 989-993.

87. Kim, P., Kim, H.Y., Kim, J. K., Reiter, G., and Suh, K. Y., *Multi-curvature liquid meniscus in a nanochannel: Evidence of interplay between intermolecular and surface forces*, **Lab on a Chip**, 2009, 9, (22), 3255-3260.
88. Eijkel, J. C. T., and van den Berg, A., *Water in micro- and nanofluidics systems described using the water potential*, **Lab on a Chip**, 2005, 5, (11), 1202-1209.
89. Haneveld, J., Tas, N. R., Brunets, N., Jansen, H. V., and Elwenspoek, M., *Capillary filling of sub-10 nm nanochannels*. **Journal of Applied Physics**, 2008, 104, (1).
90. Bowden, S. A., Wilson, R., Parnell, J., and Cooper, J. M., *Determination of the asphaltene and carboxylic acid content of a heavy oil using a microfluidic device*. **Lab on a Chip**, 2009, 9, (6), 828-832.
91. de Haas, T., Fadeai, H., and Sinton, D., *Microfluidic Characterization of Steam-Bitumen Interactions During Steam Assisted Gravity Drainage Operations*. **American Society of Mechanical Engineers**, 2013, p 681-687.
92. Fadaei, H., Shaw, J. M., and Sinton, D., *Bitumen-Toluene Mutual Diffusion Coefficients Using Microfluidics*. **Energy & Fuels**, 2013, 27, (4), 2042-2048.
93. Lesueur, D., *The colloidal structure of bitumen: Consequences on the rheology and on the mechanisms of bitumen modification*. **Advances in Colloid and Interface Science**, 2009, 145, (1-2), 42-82.

94. Bouriat, P., El Kerri, N., Graciaa, A., and Lachaise, J., *Properties of a two-dimensional asphaltene network at the water - Cyclohexane interface deduced from dynamic tensiometry*. **Langmuir**, 2004, 20, (18), 7459-7464.
95. Hibbert, O. A., *Design and Fabrication of Nanofluidic Systems for Biomolecule Characterizations*. **University of Arkansas**, 2011.
96. Bird, R. B., Stewart, W. E., and Lightfoot, E. N., *Transport Phenomena*. **Wiley**, 2007.
97. Berg, J. C., *An Introduction to Interfaces & Colloids: The Bridge to Nanoscience*. **World Scientific**, 2010.
98. Mozaffari, S., Tchoukov, P., Atias, J., Czarnecki, J., Nazemifard, N., *Effect of Asphaltene Aggregation on Rheological Properties of Diluted Athabasca Bitumen*. **Energy & Fuels**, 2015,
DOI: 10.1021/acs.energyfuels.5b00918.

APPENDIX A: MATLAB Code for Solving Equation (9)

Presented in Chapter 3

```
clear all;

clc;

gamma= 21.8*10^-3; %N/m

theta=12*pi/180;

H2=23.5*10^-9; %m

H=2*H2;

tau0=5.0; %Pa

miu=0.55*10^-3; %Pa.s

DP=-2*gamma*cos(theta)/H;

y=linspace(-H2,H2,100);

x=linspace(2*10^-4,3*10^-3,100);

%avu=tau0^3*H./(12*gamma^2*(cos(theta))^2*miu).*x.^2 -tau0*H/(4*miu)-
gamma*cos(theta)./(6*miu.*x);

ct=tau0.*x./(gamma*cos(theta));

avutt= 1/3*gamma*cos(theta)*H2./(miu.*x).*( 1-3/2.*ct+1/2.*(ct).^3 );

newavv= gamma*cos(theta)*H./(6*miu.*x);

hold on

figure(1)

%plot(x,avutt,x,newavv)

plot(x*10^3,avutt*10^3)
```

```

xx=linspace(0,3*10^-3,1000);

for i=1:1:length(xx)

xin=linspace(0,xx(i),1000);

f= 1/3*gamma*cos(theta)*H2/miu./xin .*(1- 3/2*tau0/gamma/cos(theta).*xin
+1/2.*(tau0/gamma/cos(theta).*xin).^3);

fx=1./f;

time(i)=trapz(xin,fx);

end

xnew=(gamma*cos(theta)*H/3/miu.*time).^0.5;

hold on

figure(2)

plot(sqrt(time),xx*10^3)

%plot(sqrt(time),xx,sqrt(time),xnew)

%expriment data

tex=[0.45
0.63
0.89
1.22
1.61
2
2.45
2.92
3.46
];

xex=[3.30E-01

```

4.70E-01

6.90E-01

9.68E-01

1.21

1.54

1.9

2.28

2.65

];

vex=[9.20E-01

6.46E-01

4.40E-01

3.13E-01

2.50E-01

1.96E-01

1.59E-01

1.33E-01

1.14E-01

];

hold on

figure(2)

plot(tex,xex)

hold on

figure(1)

plot(xex,vex)